Projected Changes to Cool-Season Storm Tides in the 21st Century along the Northeastern United States Coast

William James Pringle[1], Jiali Wang[1], Keith J. Roberts[2], and Veerabhadra Rao Kotamarthi[1]

[1]Argonne National Laboratory (DOE)
[2]Stony Brook University

November 24, 2022

Abstract

This study investigates changes and uncertainties to cool-season (November-March) storm tides along the U.S. northeast coast in the 21st century under the high RCP8.5 emission scenario compared to late 20th century. A high-fidelity (50-m coastal resolution) hydrodynamic storm tide model is forced with three dynamically-downscaled regional climate models (RCMs) over three decadal periods (historical, mid-21st century and late-21st century) to project future changes in peak storm tide elevations at coastal counties in the region. While there is no absolute consensus on future changes to storm tides, for any one future decade two out of the three RCMs project an increase at counties along the Hudson River, Delaware River and northern Chesapeake Bay due to more intense cyclones that track inland of these locations leading to favorable surge generating conditions. The same RCMs also project a decrease at counties facing the open ocean in the mid-Atlantic Bight as cyclone densities just offshore of the coastline decrease, particularly by late-century. The larger tidal range in northern areas leads to significant uncertainty due to the arbitrary relationship between the local tidal stage and when a surge event occurs, which affects both the magnitude and sign of the projected changes. This tide-surge timing is less important in the Chesapeake Bay and unimportant in Albemarle Sound and Pamlico Sound. Similar to other recent studies, we highlight that sea level rise is likely to be more critical than storm climatology for future changes to the cool-season coastal flooding potential.

Projected Changes to Cool-Season Storm Tides in the 21st Century along the Northeastern United States Coast

William J. Pringle[1], Jiali Wang[1], Keith J. Roberts[2], Veerabhadra R. Kotamarthi[1]

[1]Environmental Science Division, Argonne National Laboratory, Lemont, IL, USA
[2]School of Marine and Atmospheric Science, Stony Brook University, NY, USA

Key Points:

- Cool-season storm tides projected to decrease along the Mid-Atlantic Bight coast but increase further inland up estuaries and rivers.
- Arbitrary tide-surge timing strongly affects projected storm tide changes in New England, New York-New Jersey Bight, and Delaware Bay.
- Sea level rise is likely to be more critical than storm climatology to future changes in cool-season coastal flooding potential.

Corresponding author: William Pringle, `wpringle@anl.gov`

Abstract

This study investigates changes and uncertainties to cool-season (November-March) storm tides along the U.S. northeast coast in the 21^{st} century under the high RCP8.5 emission scenario compared to late 20^{th} century. A high-fidelity (50-m coastal resolution) hydrodynamic storm tide model is forced with three dynamically-downscaled regional climate models (RCMs) over three decadal periods (historical, mid-21^{st} century and late-21^{st} century) to project future changes in peak storm tide elevations at coastal counties in the region. While there is no absolute consensus on future changes to storm tides, for any one future decade two out of the three RCMs project an increase at counties along the Hudson River, Delaware River and northern Chesapeake Bay due to more intense cyclones that track inland of these locations leading to favorable surge generating conditions. The same RCMs also project a decrease at counties facing the open ocean in the mid-Atlantic Bight as cyclone densities just offshore of the coastline decrease, particularly by late-century. The larger tidal range in northern areas leads to significant uncertainty due to the arbitrary relationship between the local tidal stage and when a surge event occurs, which affects both the magnitude and sign of the projected changes. This tide-surge timing is less important in the Chesapeake Bay and unimportant in Albemarle Sound and Pamlico Sound. Similar to other recent studies, we highlight that sea level rise is likely to be more critical than storm climatology for future changes to the cool-season coastal flooding potential.

Plain Language Summary

Winter storms (e.g., nor'easters) that develop during the North American cool-season (November to March) can generate high water levels (storm tides) along the northeast coast of the U.S that can potentially result in coastal flooding. This study is concerned with how winter storm tides along the northeastern U.S. coast could change into the 21^{st} century under a high emissions climate change scenario. Highly-resolved computer models of the ocean and the atmosphere are used to investigate this question. We find that changes to storm tides are generally less significant than expected sea level rise under the corresponding climate change scenario. However, we find evidence of decreasing storm tides at counties along the Mid-Atlantic Bight coastal region and increasing storm tides at counties along the Hudson River, Delaware River and northern Chesapeake Bay. Expected changes to storm tides are more uncertain in northern areas (New England, Long Island Sound, New York Bight, and Delaware Bay) because of the random timing of the storm and the everyday tide level, which is larger in these areas. Coastal planning should consider the combination of sea level rise and storm tides taking into account the full range of possibilities based on this random tide-storm timing.

1 Introduction

Storm surges along the northeastern coast of the United States (herein NEC) are frequently generated by the strong low-level winds and low surface pressures of extratropical cyclones (ETCs) that often develop during the North American cool-season months (November to March) (Colle et al., 2013; Booth et al., 2016; Catalano & Broccoli, 2018). Depending on the timing of the surge in relation to the astronomical tide, the resultant storm tide elevation can lead to coastal flooding, in addition to otherwise hazardous marine conditions. Some noteworthy events include the December 27, 2010 nor'easter that induced a ~1-m surge which coincided with high tide causing extensive flooding in Scituate, Massachusetts (Beardsley et al., 2013); and the December 11-12, 1992 nor'easter generated a 1-1.5-m surge around New York City and western Long Island that lasted over three tidal cycles (Colle et al., 2008). The storm tide elevation eventually reached ~2.5-m above mean sea level during high tide at lower Manhattan, resulting in flooding to New York City's subways and train systems (Colle et al., 2010).

While often less severe than hurricane-driven surge, ETCs are responsible for most moderate surge events in the NEC region and affect a very wide region of the coastline (Booth et al., 2016). It is thus important to assess the impacts of ETC-driven surge and storm tides, especially when considering events of moderate frequency (1- to 3-year timescales). Systematic changes to ETCs under a changing climate could affect the frequency and severity of cool-season storm tides leading to more (or less) frequent coastal flooding. For instance, it has been shown that large ETC-driven surges along the NEC are typically generated by slow-moving deep cyclones to the south of a strong anticyclone (Catalano & Broccoli, 2018), so changes in these types of events would be play a critical role in altering the frequency of ETC-driven coastal flooding events. Furthermore, any changes to storm tides must be viewed with respect to rising sea levels that would further enhance the risk to coastal flooding (Booth et al., 2016), so it is also important to put the magnitudes of each into context.

Several studies have explored the effects of global warming on cool-season ETC climatology for the NEC. Most of these project a reduction in the density of ETCs over the continental United States and western North Atlantic Ocean (Teng et al., 2008; Long et al., 2009; Chang, 2013; Colle et al., 2013; Seiler et al., 2018). ETC intensities over the western North Atlantic Ocean are also predicted to weaken, however cyclones may become more intense and deepen more rapidly just inland of the NEC (Colle et al., 2013). Many of these studies used output from global climate models (GCMs), particularly those from phase 5 of the Coupled Model Intercomparison Project (CMIP5; Taylor et al., 2012) which have horizontal model resolutions of ∼100-300 km. Due to the regional differences and dependence on model resolution, Colle et al. (2013) suggests that dynamically downscaled regional versions of the GCMs are needed to investigate the changes to ETC track density and intensification in more detail. Other studies show that 20-km horizontal resolution dynamically downscaled regional climate models (RCMs) generate stronger cyclones than the parent GCMs based on the surface wind speed (Booth et al., 2018; Zhang & Colle, 2018). The downscaled simulations also indicated that latent heating related diabatic processes, which are otherwise too weak in coarse-resolution GCMs, could enhance development of intense ETCs over the NEC (Zhang & Colle, 2018). However, studies by Long et al. (2009); Seiler et al. (2018) suggest that projected changes to ETC density are not particularly sensitive to model resolution.

Previous studies have examined climate change impacts on cool-season surge along the NEC using statistical (Roberts et al., 2017) or hydrodynamic (Lin et al., 2019) surge models forced by surface winds and pressure from CMIP5 GCM ensembles. Roberts et al. (2017) found no significant change to surge return intervals in a future period (2054-79) compared to a historical period (1974-2004) at The Battery in New York City. This was attributed to the fact that projected ETC changes did not occur in regions that favor the generation of surge at The Battery. Similarly, Lin et al. (2019) found relatively small projected changes (<7%) to extreme storm surge heights for the same future period along most of the NEC, while noting however that one of the GCMs showed a more substantial increase of up to 36% for the 50-year surge height. These previous analyses contain uncertainties due to the usage of atmospheric forcings from coarsely resolved GCMs and surge prediction by straightforward multilinear regression (Roberts et al., 2017) or a relatively coarse resolution hydrodynamic model (∼1-km coastal resolution; Lin et al., 2019). Furthermore, astronomical tides were omitted even though it is the combination of surge and tide (storm tide) that needs to be considered to assess local flooding potential (Horsburgh & Wilson, 2007). In this study, we address these limitations by integrating results from three 12-km dynamically downscaled RCMs with a high-fidelity (∼50-m coastal resolution) hydrodynamic storm tide model, which we run multiple times to account for the arbitrary surge-tide phasing. Using this high-resolution integrated modeling system we aim to: 1) quantify projected changes and associated uncertainties of cool-season storm tides in the 21^{st} century along the NEC as compared to estimates of

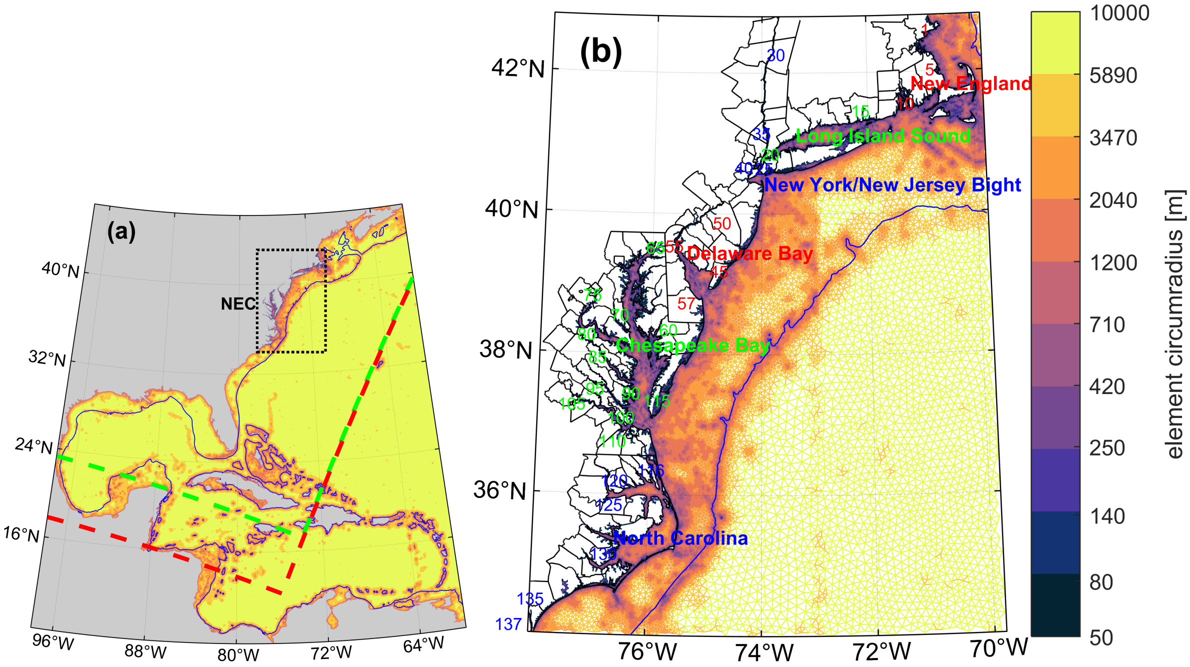

Figure 1. Computational domain and unstructured mesh resolution of the ADCIRC hydrodynamic storm tide model. (a) Full extent of the computational domain covering the western North Atlantic Ocean. The blue line demarcates the 200-m depth contour – approximate edge of the continental shelf. Dashed outlines indicate the boundary of the WRF-based regional climate models used to force the storm tide model (WRF-CCSM4: green, WRF-GFDL/HadGEM: red). The dashed black box indicates the NEC region that is shown in more detail in panel (b). Coastal counties (partially numbered in this figure; see spreadsheet datasets in Pringle (2020) for full county numbering and metadata) are demarcated by the black outlines. The colored labels (corresponding to proximate counties of the same color) indicate locations of the different sub-regions focused on in this study.

sea level rise (SLR), and 2) relate projected storm tide changes to the ETC climatology, such as changes to track patterns and intensity.

The rest of this paper is organized as follows: first we introduce the modeling and analysis approach in Sect. 2; in Sect. 3 we present results showing model accuracy during the historical period, followed by our projected changes to storm tides in future decades and the associated ETC patterns driving these storm tide changes; in Sect. 4 we discuss our major findings and their implications, as well as the uncertainties and limitations of the study.

2 Methods

2.1 Dynamically Downscaled Regional Climate Model Experiments

Three sets of CMIP5 GCMs (CCSM4, GFDL-ESM2G and HadGEM2-ES) have been dynamically downscaled to 12 km horizontal resolution using the Weather Research and Forecasting (WRF) v3.3.1 model (Wang & Kotamarthi, 2015; Zobel et al., 2018). These three GCMs were chosen based on evidence that they approximately represent the spread of climate sensitivity for the 30 GCMs in the CMIP5 experiment (GFDL-ESM2G – lower sensitivity, CCSM4 – moderate sensitivity, HadGEM2-ES – high sensitivity) (Sherwood et al., 2014; Zobel et al., 2018). Herein, the downscaled RCMs are referred to as WRF-CCSM4, WRF-GFDL and WRF-HadGEM. The WRF computational domains cover all of the continental USA (see Fig. S1) extending out to the western North Atlantic Ocean to encompass all of the U.S. East Coast and Gulf Coast, and parts of the Caribbean (Fig. 1). Sea level pressures (SLP) and 10-m wind velocities (U10; both zonal and meridional directions) are output from the model simulations at 3-hourly intervals and used to forced the hydrodynamic storm tide model.

Each RCM provides meteorological data for three decadal periods; 1995-2004 ("historical" decade), 2045-2054 ("mid-century" decade), and 2085-2094 ("late-century" decade). This corresponds to nine continuous cool-seasons for each decade, e.g., November 1995-March 1996 to November 2003-March 2004 for the historical decade. The future decades were simulated under the Representative Concentration Pathway (RCP) 8.5, a pathway that assumes high levels of greenhouse gas emissions by 2100 with an effective radiative forcing increase of 8.5 W/m^2 due to a large global population and little technological improvement (Riahi et al., 2011). Recent estimates predict that RCP8.5 will accurately represent current emissions out until mid-century and represents at least plausible levels out until late-century (Schwalm et al., 2020).

2.2 Hydrodynamic Storm Tide Model

The ADvanced CIRCulation (ADCIRC) hydrodynamic model (Luettich & Westerink, 2004) is used to simulate storm tides along the NEC. We use Version 55 of the model that newly incorporates self-attraction and loading (SAL) tides, internal tide induced wave drag, and modifications to the governing equations to correctly account for Earth's curvature (Pringle et al., 2020). The ADCIRC computational domain covers the western North Atlantic Ocean west of the 60° meridian (Fig. 1a), a well-studied region for the ADCIRC model (e.g., Westerink et al., 2008; Bunya et al., 2010; Hope et al., 2013; Marsooli & Lin, 2018; Roberts, Pringle, Westerink, Contreras, & Wirasaet, 2019). Version 3 (Pringle & Roberts, 2020) of OceanMesh2D (Roberts, Pringle, & Westerink, 2019) is used to automatically generate an unstructured mesh for the study domain using carefully designed combinations of shoreline geometry and seabed topography-based element sizing functions (cf. Roberts, Pringle, Westerink, Contreras, & Wirasaet, 2019). A nominal minimum element size concentrated at the coast is set to 50 m in the NEC region and 1 km elsewhere (Fig. 1). The nominal maximum element size in the deep ocean is set to 10 km. Mesh bathymetry is interpolated from the high-resolution (~1-3-m) USGS Coastal National Elevation Database (CoNED) in the NEC region and ~500-m SRTM15+ (Tozer et al., 2019) Version 2 data elsewhere.

The storm tide model is forced with SLP and U10 (both zonal and meridional directions) from the downscaled WRF climate model data, in addition to astronomical tidal potential and SAL for the eight dominant tidal constituents (M_2, S_2, N_2, K_2, K_1, O_1, P_1, Q_1). Astronomical tides are also prescribed at the open boundary using the TPXO9-Atlas (Egbert & Erofeeva, 2019). To account for the random timing between tides and storm-driven surge we simulate each season five times with different tidal phases (-10, -5, +0, +5, +10 hour offsets from the actual date-time). A computational time step of 12 s was used for all simulations, and water elevations were output at 1 hour intervals for the analysis.

2.3 Peak Storm Tide Elevations

For each decade and each realization of the five tidal phases we extracted Peak Storm Tide elevations (PST) separated by a minimum of 3 days from the data to identify unique ETC-driven events (Lin et al., 2019). In previous studies this data has been processed into extreme value estimates of low frequency PST events, e.g., 50-year and 100-year return periods, obtained by fitting the tail of extracted peaks to the Generalized Pareto

Distribution using the Peak Over Threshold method (Lin et al., 2019; Marsooli et al., 2019). However, we deemed the decadal-long simulations in this study to be too short to conduct a robust extreme value analysis. We instead choose to measure changes in PST for return periods contained within the time period of the simulations; the 3-season and 1-season return periods. We define the 3-season PST empirically as the third highest PST within a decade (i.e., the third largest in nine cool seasons); while the 1-season PST is defined as the ninth highest PST within a decade.

Simulated PST values are reduced to a single value for each county along the NEC coast (Fig. 1) so that the results are more easily presented and understood (these results are described in Sects. 3.2-3.3). The value for each county is taken as the maximum PST at the mesh vertices along the coastline of that county (c.f. Marsooli et al., 2019). For comparison, the astronomical MHHW (mean higher high water) value for each county is also approximated from harmonic constituent amplitudes ($\approx 1.1M_2{+}K_1{+}O_1$ – half of the sum of the mean range and diurnal range, Parker, 2007). Differences in the county-wide PST values between future and historical decades are presented individually for each RCM forcing. The tidal phase related uncertainty in the difference is found by taking the minimum, mean and maximum differences of all possible combinations of tidal phase in the future and historical decade (25 total).

Furthermore, we compare the relative magnitude of storm tide changes to SLR under the RCP8.5 scenario, which is computed for each county from the ocean model outputs of the three parent GCMs. SLR is approximated as the difference between the future cool-season decadal average and the historical cool-season decadal average of the total sea surface height in the closest GCM ocean point to the county midpoint. We define the total sea surface height as the sea surface height (CMIP5 variable *zos*) plus the global average steric sea level change (CMIP5 variable *zossga*) (Becker et al., 2016)

2.4 Cyclone Tracking and Mapping to Peak Storm Tides

To attribute changes in storm tides to patterns of ETC tracks and intensities, we extracted storms from the meteorological data by tracking the local minimums of SLP using Version 2 of CycloneTrack (Flaounas et al., 2014), a cyclone tracking algorithm. To filter out small scales in SLP a 2-D Gaussian smoothing kernel with a standard deviation of 10 is used.

We select ETC tracks that produce a large peak storm tide elevation within one of the following six multi-county subregions: New England (NE), Long Island Sound (LIS), New York/New Jersey Bight (NY/NJ), Delaware Bay (DB), Chesapeake Bay (CB), and North Carolina (NC) (Fig. 1). Tracks are selected by finding those that exist within the NEC domain just before and after the time of the peak storm tide. Usually there is just one track that meets this criteria, but sometimes there are no tracks in which we skip to the next highest peak storm tide elevation, or very occasionally there are two tracks in which we record both. Using this methodology, in Sect. 3.4 we present the ETC tracks from the nine highest PST for each RCM for each subregion.

3 Results

3.1 Historical Decade Model Accuracy

3.1.1 Dynamically Downscaled Regional Climate Model

Figures showing the historical accuracy of the WRF-based RCM simulations compared to offshore buoy observations and ERA5 reanalysis data (European Centre for Medium-Range Weather Forecasts, 2019) are presented in the supplementary material. Low-level winds in the RCMs during the historical decade are shown to be mostly accurate (RMSE < 0.6 m/s) at offshore buoy locations and in the northern part of the NEC region, while errors are largest (RMSE up to 2.4 m/s) near the North Carolina and Virginia coastline (Fig. S2). Higher errors at the coast could be due to land-masking and geopotential height discrepancies in the WRF model. There is a tendency for southeasterly-southwesterly winds speeds to be overestimated and westerly-northwesterly wind speeds to be slightly underestimated throughout the region (Fig. S3-S5).

Compared to ERA5, the density distribution of simulated ETCs in the NEC region are shown to be accurate to within 1-2 cyclones/season for all the RCMs (Fig. S6), showing improvements over the parent GCMs which tend to underestimate cyclone densities further (Roberts, 2015). WRF-CCSM4 underestimates the density of ETCs offshore while WRF-HadGEM overestimates. WRF-GFDL overestimates cyclone density closer to the coast especially near the New Jersey and New York region. Compared to ERA5, WRF-CCSM4 shows good agreement in the shape of the distribution of ETC maximum lifecycle intensities [minimum SLP (Pmin) and maximum U10 (Umax)], but it produces too few of the most frequently observed cyclones (Pmin $\sim$990-1010 hPa, Umax $\sim$14-24 m/s; Fig. S7). The WRF-GFDL and WRF-HadGEM produce a greater overall number of ETCs than WRF-CCSM4, which matches more closely with ERA5 (Fig. S7). However, there are more ETCs of greater intensity (Pmin $<$ 990, Umax $>$ 24 m/s) than in ERA5. Similarly, Figs. S3-S5 show that the 95% quantile wind speeds against offshore buoys are more overestimated in WRF-GFDL and WRF-HadGEM RCMs than in WRF-CCSM4.

3.1.2 Hydrodynamic Storm Tide Model

The historical accuracy of the hydrodynamic storm tide model simulations have been assessed based on computing root-mean-square errors (RMSE) from quantile-quantile plots of daily maximum water levels (DMWL). Errors are within 0.2 m throughout most of the NEC (Fig. 2); the tidal range at one tide gauge in a complex wetland environment (Wachapreague, VA) is overestimated by the model leading to the highest errors there (RMSE $\sim$ 0.3 m). The errors of the RCM-forced runs are distributed similarly to those under the ERA5 reanalysis forcing, partly because both surge and tidal components contribute to the DMWL. The greatest difference in DMWL errors between the atmospheric forcings is found in Delaware Bay and Chesapeake Bay. Wind speed errors (Fig. S2) just offshore of Delaware Bay and Chesapeake Bay were shown to be largest for the WRF-HadGEM model which could be contributing to the also generally larger associated DMWL errors in these estuaries. Wind speed errors inside Chesapeake Bay is greatest for WRF-CCSM4 and associated DMWL errors throughout Chesapeake Bay are indeed larger than those under ERA5 and WRF-GFDL forcing.

The simulated 3-season PST (mean of the five tidal phase realizations) during the historical decade at each mesh vertex in the NEC region under ERA5 reanalysis and RCM forcing is shown in Fig. 3. Furthermore, the 3-season and 1-season PST are compared to selected NOAA tide gauges in the NEC region in Fig. 4 using error bars to indicate the tidal phase-based uncertainty, whereas the observational data (demeaned for each season) is a single realization of the tidal phase. This uncertainty is greater for the lower frequency 3-season PST (Fig. 4a) than the 1-season one (Fig. 4b), and is greatest along the stretch of coastline from Woods Hole to Atlantic City tide gauges under WRF-GFDL forcing. Although the spatial distribution of PSTs are similar under all meteorological forcing since it is heavily related to the tidal range, the RCM forcing consistently generates greater storm tide elevations than the reanalysis forcing. The RCM-forced PSTs are indeed overestimated at some tide gauges, in particular those in the Long Island Sound and Delaware Bay (Woods Hole to Montauk, Philadelphia and Reedy Point). However, it is equally true that PSTs under reanalysis forcing are underestimated at many of the tide gauges, which could mean that the most extreme winds are smoothed-out in the reanalysis data compared to the RCMs.

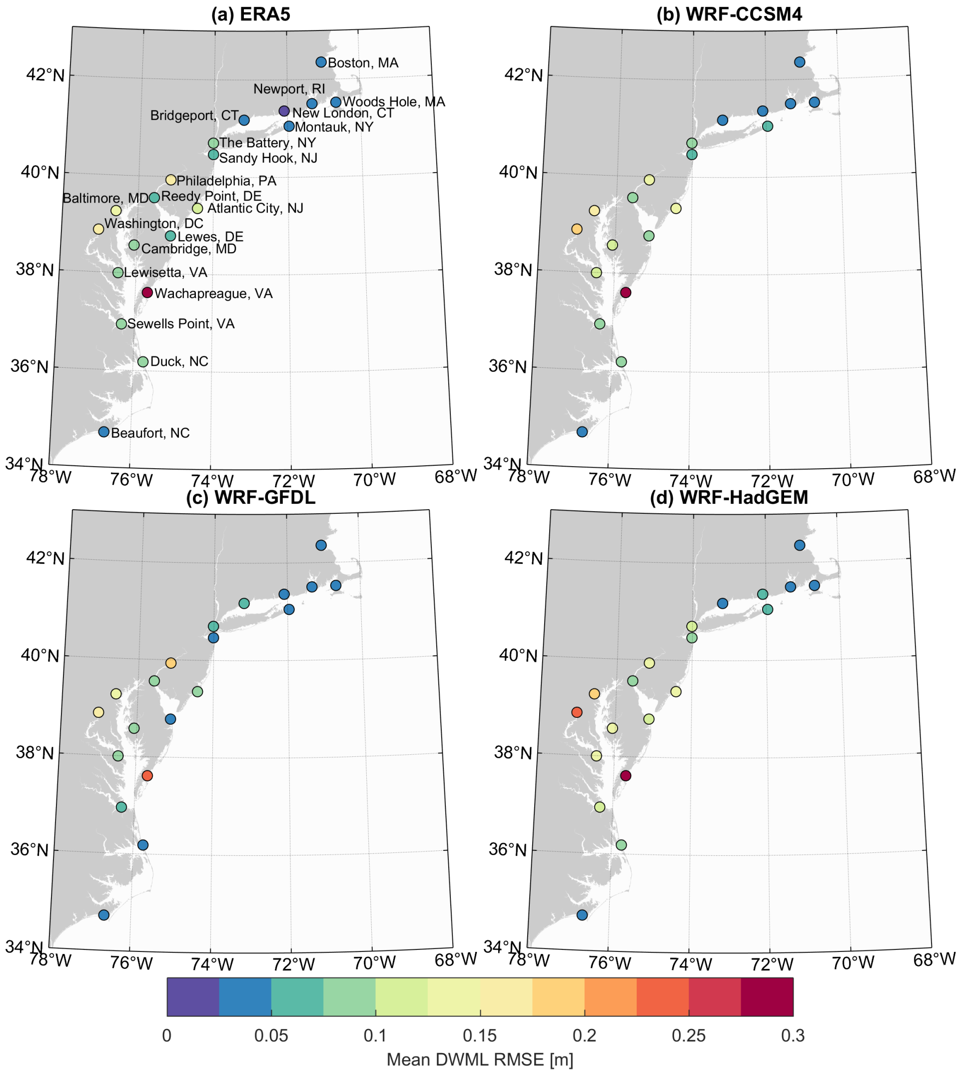

Figure 2. Accuracy (mean RMSE from the five tidal-phase realizations) of daily maximum water levels (DMWL) simulated by the hydrodynamic model at NOAA tide gauges in the NEC region for the historical cool-season decade (1995-2004). The hydrodynamic model was driven by atmospheric forcing from (a) ERA5 reanalysis, (b) WRF-CCSM4, (c) WRF-GFDL, (d) WRF-HadGEM.

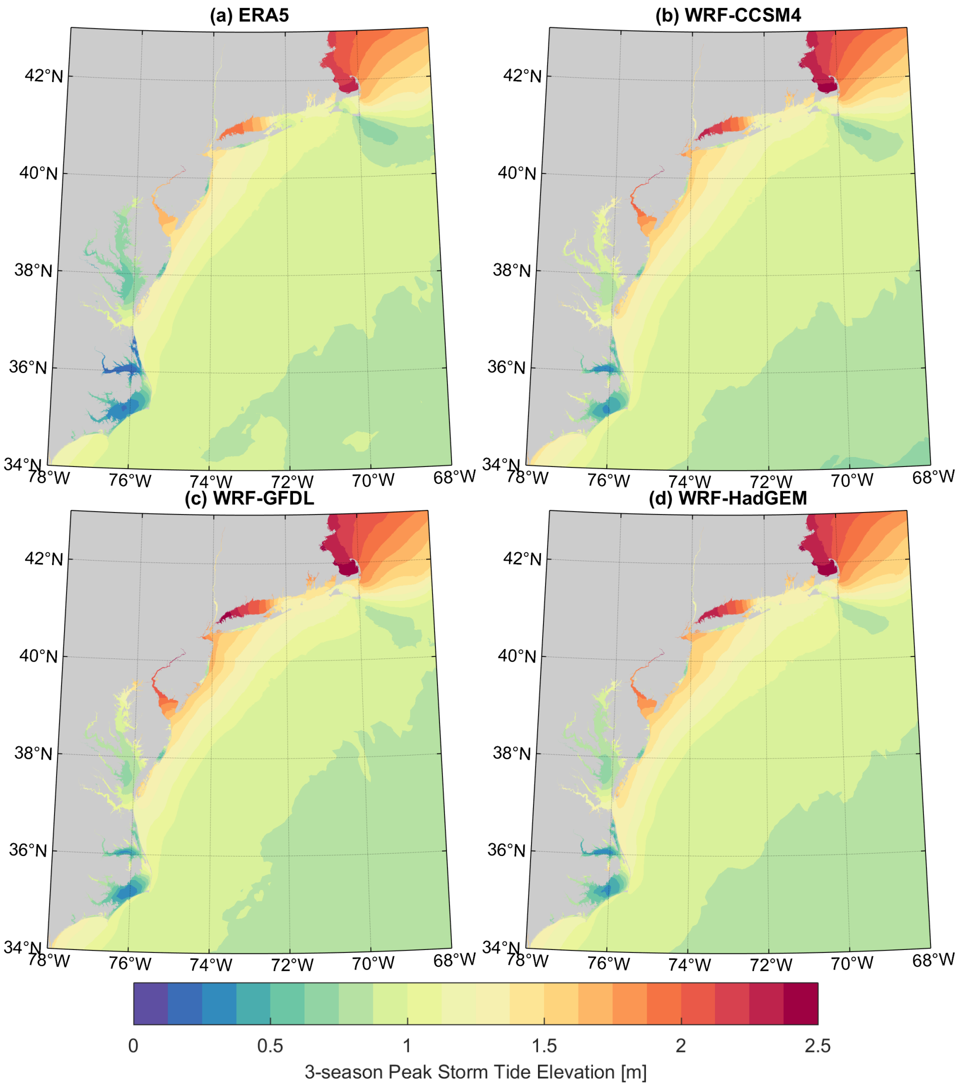

Figure 3. Comparison of the hydrodynamic model simulated 3-season PST (peak storm tide elevation) in the NEC region for the historical cool-season decade (1995-2004). Results shown are the mean of the five tidal phase realizations simulations for each meteorological forcing: (a) ERA5 reanalysis, (b) WRF-CCSM4, (c) WRF-GFDL, (d) WRF-HadGEM.

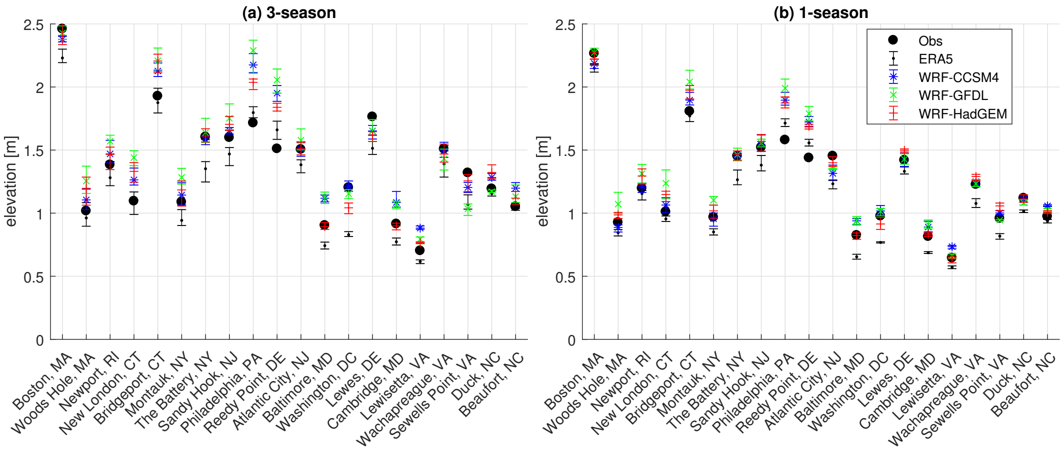

Figure 4. Comparison of observed and simulated (a) 3-season and (b) 1-season PST (peak storm tide elevations) at NOAA tide gauges in the NEC region (locations shown in Fig. 2) for the historical cool-season decade (1995-2004) under various meteorological forcing. The error bars indicate the mean and upper/lower bounds for the five tidal phase realizations.

3.2 Peak Storm Tide Elevation Changes in Mid-Century Decade

Projected PST changes range within ±0.4 m for the 3-season PST (Fig. 5b) and ±0.3 m for the 1-season PST (Fig. 6b) throughout the NEC region for the three RCM forcings by mid-century. The magnitude of the 3-season PST changes by mid-century across the NEC are of similar order to SLR under the CCSM4 and GFDL SLR scenarios (∼0.2 m). However, the magnitude of SLR according to HadGEM (0.6-0.8 m) is significantly larger than 3-season PST changes. The magnitude of 1-season PST changes by mid-century across the NEC are slightly smaller in magnitude to CCSM4/GFDL SLR (∼0.2 m), and much smaller than HadGEM SLR (0.6-0.8 m).

In the northern counties (<#60) projected PST changes are highly dependent on the RCM forcing. WRF-CCSM4 forcing results in mostly small average (tidal phase-based) increases to PSTs in the New England, Long Island Sound, and New York/New Jersey Bight subregions and up to as large as 0.15 m along the Delaware River (#47-55) in the Delaware Bay subregion. Similarly, WRF-HadGEM forcing projects on average mostly small increases to the 3-season PST, where larger increases up to 0.2 m are recorded throughout most of the New York/New Jersey Bight subregion, at Rhode Island counties (#10-14) in the New England subregion, and at counties along the Delaware River. For the 1-season PST, WRF-HadGEM projects mostly little change but localized increases (∼0.1 m) for counties along the Hudson River (#30-34), and decreases (0.05-0.15 m) for counties #40-45 and #56-58, which are located along the New Jersey coastline and at the entrance to Delaware Bay, facing the open ocean. In contrast, the WRF-GFDL run shows an average decrease to PSTs at all of the northern counties at magnitudes of 0.1-0.3 m for the 3-season and ∼0.1 m for the 1-season. The tidal phase-based variability of these changes in these northern counties is comparatively large at 0.3-0.5 m for the 3-season PST and 0.15-0.3 m for the 1-season PST under all RCMs, which is larger than most of the tidal phase-based average changes.

For southern counties (>#60), WRF-CCSM4 and WRF-HadGEM forcings largely project average decreases. While little change to PSTs is seen in the central west regions of Chesapeake Bay (counties #60-90), fairly large average decreases are projected under these two RCM forcings elsewhere, up to 0.2 m-0.3. Comparatively, the WRF-GDFL run projects mostly small average increases to PSTs of ∼0.2 m for 3-season and ∼0.1

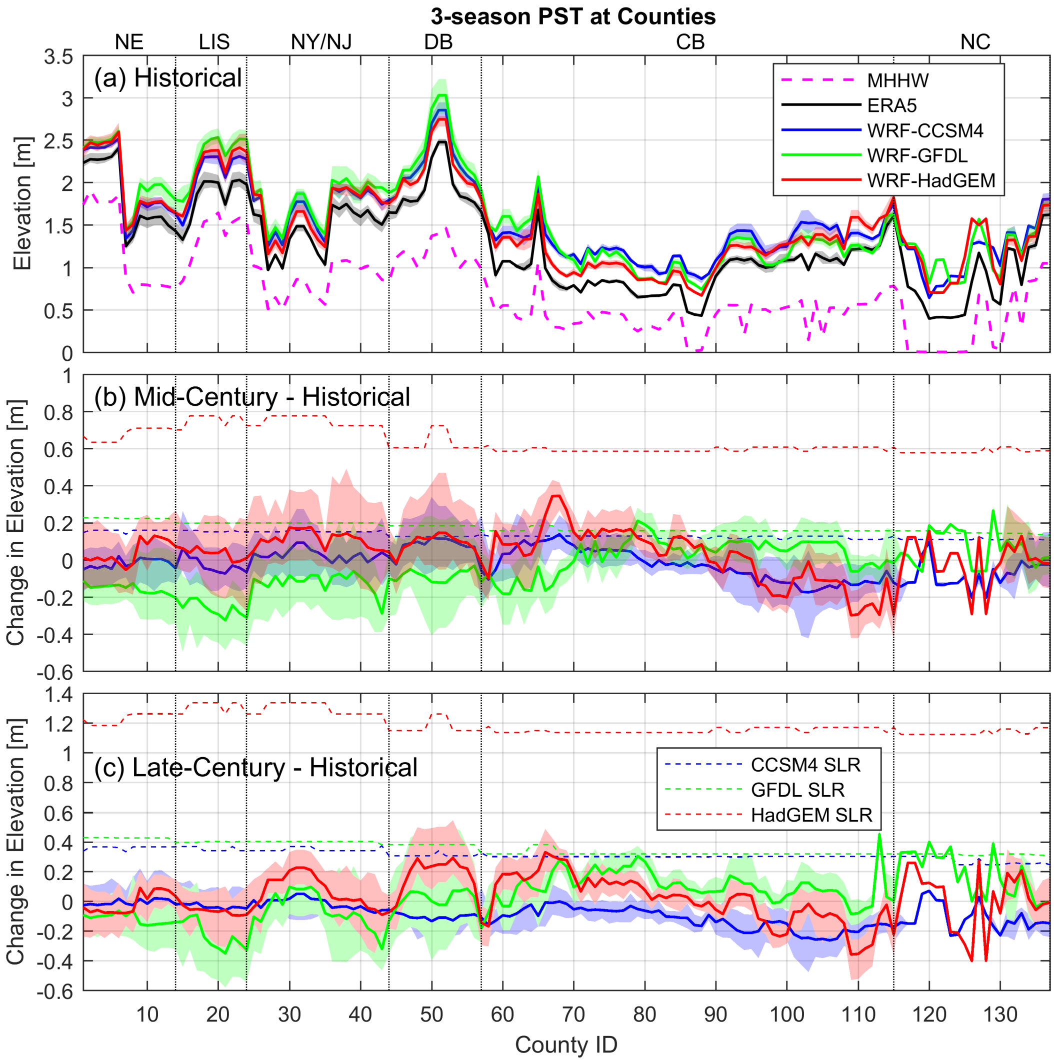

Figure 5. Simulated 3-season PST (peak storm tide elevations) at counties along the NEC coastline (see Fig. 1 for locations) during the cool-season under various meteorological forcing). (a) Historical decade (1995-2004) including the modeled astronomical MHHW, (b) Mid-century decade (2045-2054) minus historical decade, (c) Late-century decade (2085-2094) minus historical decade. Solid lines show the tidal phase-based mean and the translucent bands show the tidal phase-based range. The dashed lines in (b) and (c) indicate the decadal mean increase in sea level (SLR) compared to the historical decade for the parent GCMs. NE: New England, LIS: Long Island Sound, NY/NJ: New York/New Jersey Bight, DB: Delaware Bay, CB: Chesapeake Bay, NC: North Carolina.

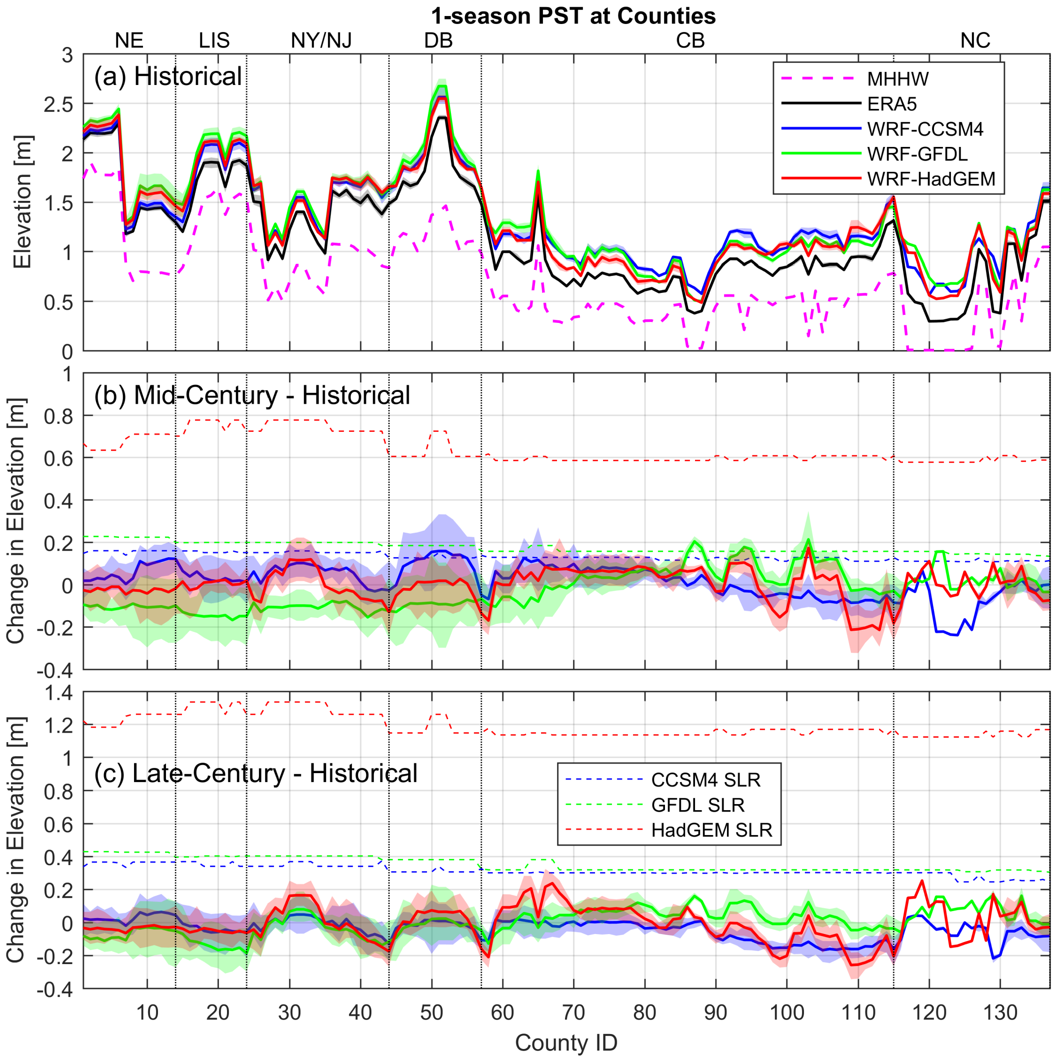

Figure 6. Same as Fig. 5 but for 1-season PST.

m for the 1-season in these southern counties. Localized larger average increases of ∼0.15-0.2 m to the 1-season PST are noticeable at counties located up western tributaries of Chesapeake Bay and Albemarle Sound (#86-88, #94-95, #103, #121-122). The tidal phase-based variability is not very significant for these southern counties, especially for those in the north part of the North Carolina subregion. This area corresponds to Albemarle and Pamlico Sounds that have a tidal range of only a few centimeters (refer MHHW in Fig. 5a), and hence susceptible to changes in PST due to locally generated storm surge only.

3.3 Peak Storm Tide Elevation Changes in Late-Century Decade

Projected PST changes range within ±0.5 m for the 3-season PST (Fig. 5c) and ±0.3 m for the 1-season PST (Fig. 6c) throughout the NEC region for the three RCM forcings by late-century. In this decade the WRF-GFDL and WRF-HadGEM forcings project changes that have a high-degree of spatial variability, while WRF-CCSM4 shows smaller and smoother changes. The magnitude of the 3-season PST changes in late-century across the NEC are similar to but mostly smaller in magnitude to SLR under the CCSM4 and GFDL SLR scenarios (∼0.4 m). The magnitude of SLR according to HadGEM (1.1-1.3 m) is far greater than the 3-season PST changes; it is at least two times the size of the greatest PST decrease for any run and county. The magnitude of the 1-season PST changes by late-century across the NEC are all smaller (at least slightly) in magnitude to CCSM4/GFDL SLR (∼0.4 m), and are completely dwarfed by HadGEM SLR (1.1-1.3 m).

In the northern counties (<#60), WRF-CCSM4 forcing projects only very small average (tidal phase-based) changes to the 3-season PST in the New England, Long Island Sound, and New York/New Jersey Bight subregions and a decrease of ∼0.1 m in the Delaware Bay subregion. Also under WRF-CCSM4 forcing, the 1-season PST is mostly unchanged in these northern counties except for a decrease of ∼0.1 m for counties near the entrance to Delaware Bay (#44 and #58) facing the open ocean. In most of the northern counties, WRF-HadGEM forcing projects very small average changes to the 3-season PST, however there are large increases (∼0.2-0.3 m) along the Hudson River (#30-33) and Delaware River (#47-55). For the 1-season PST, WRF-HadGEM projects average increases of 0.15-0.25 m at counties along the Hudson River and average decreases of ∼0.2 m for counties near the entrance to Delaware Bay (#44 and #58) facing the open ocean (also true for WRF-GFDL). Comparatively, WRF-GFDL forcing projects mostly average decreases to PSTs for northern counties (up to 0.35 m for the 3-season and 0.2 m for the 1-season). However, there are increases, although smaller (<0.1 m) than for WRF-HadGEM, at the same Hudson River and Delaware River counties.

For the southern counties (>#60), WRF-GFDL projects mostly increases to PSTs – up to 0.5 m for the 3-season but only up to 0.15 m for the 1-season – and WRF-CCSM4 projects mostly decreases – up to 0.25 m for the 3-season and 0.15 m for the 1-season. WRF-HadGEM forcing shows more spatial variability to projected PST changes. For instance, WRF-HadGEM projects average increases to the 1- and 3-season PSTs of 0.15-0.3 m at northern Chesapeake Bay (#63-69), and northern Albemarle Sound (#117-119) counties, but average decreases of up to 0.25-0.3 m at counties in the southwest portion and at the entrance of Chesapeake Bay (#96-115). There is no RCM-wide consensus in the North Carolina subregion with average changes ranging from 3-season PST decreases up to 0.4 m for WRF-HadGEM to increases of 0.4 m for WRF-GFDL. The same is true for 1-season PST changes but the variation between RCM forcings is smaller in magnitude (±0.2 m).

3.4 Cool-season Storm Climatology Patterns Driving Storm Tide Changes

In the northern subregions (New England, Long Island Sound, New York/New Jersey Bight) during the historical period, many of the RCM-simulated highest nine peak storm tide generating ETC tracks tend to follow nearby and parallel to the coastline (Figs. 7). In the future decades ETC tracks tend to be more sparsely distributed and are less likely to follow that coastline parallel track, either veering further offshore or tracking more inland in the south-to-north direction. Specifically, in WRF-GFDL there are fewer storms that make close or direct impact to the subregion of concern which could explain why WRF-GFDL forced PSTs are projected to mostly decrease in the northern subregions in future decades. However, WRF-GFDL forced PSTs are projected to increase in the Hudson River in the late-century decade. It is noticeable that all WRF-GFDL decades produce storms that pass through the northern New York/New Jersey Bight subregion where Hudson River is located, but in the late-century the storm tracks are clustered further to the north than the other two decades. Due to the anticlockwise cyclone rotation, southerly winds which would be favorable to surge generation in the river are to the southeast of the cyclone center. Similarly, WRF-HadGEM shows a number of relatively intense storms tracking just inland of the Long Island Sound and New York/New Jersey Bight subregions in the south-to-north direction in future decades, particularly in the mid-century. Future PSTs under WRF-HadGEM forcing are largely increased in the Hud-

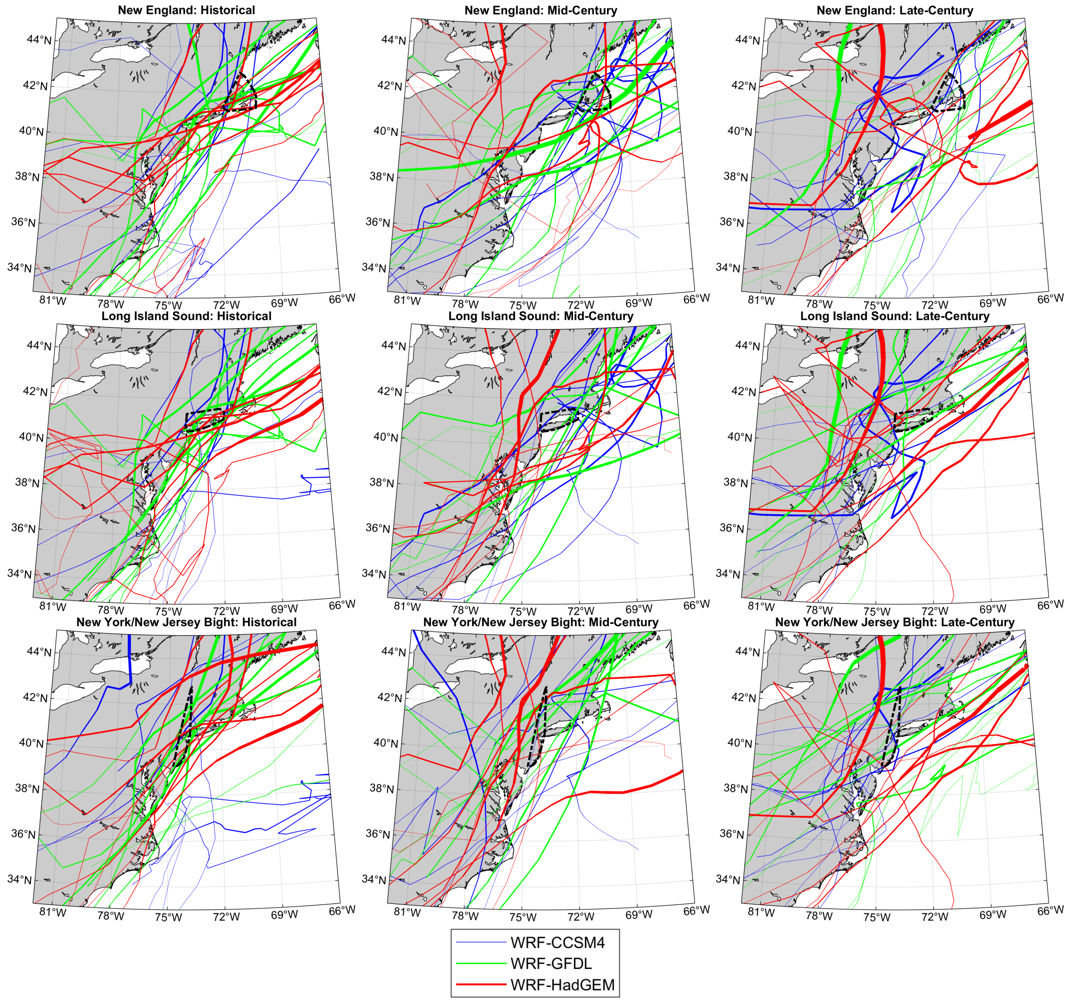

Figure 7. Distribution of regional climate model (RCM)-simulated cool-season ETC tracks that produce the nine highest peak storm tide elevations under each RCM forcing within a northern subregion as indicated by the black dashed-line polygon (top: New England, middle: Long Island Sound, bottom: New York/New Jersey Bright). The tracks are color coded according to the RCM and line thicknesses are proportional to ETC intensity (Pmin, lower is thicker). Tracks are shown for the three decades investigated in this study (left-to-right): Historical (1995-2004), Mid-century (2045-2054), and Late-century (2085-2094).

son River as well as in west New England and east Long Island Sound counties for the 3-season PST. In the historical period most WRF-HadGEM storms generating surge in the New England and Long Island Sound subregions passing to just offshore at southwest-to-northeast direction which are likely not as favorable to generating surge as storms that track further inland in the south-to-north direction. The WRF-CCSM4 RCM meanwhile shows more storms passing through or close to the subregions in the future decades than the historical one, and the storms are somewhat more intense. WRF-CCSM4 forcing showed increases to the 1-season PST in both future decades (greater increase in the mid-century) at the west New England and Hudson River counties. However, the WRF-CCSM4 storms are not as intense as some of those in future WRF-GFDL/WRF-HadGEM simulations, potentially explaining why the lower frequency 3-season PST under WRF-CCSM4 forcing is largely unchanged.

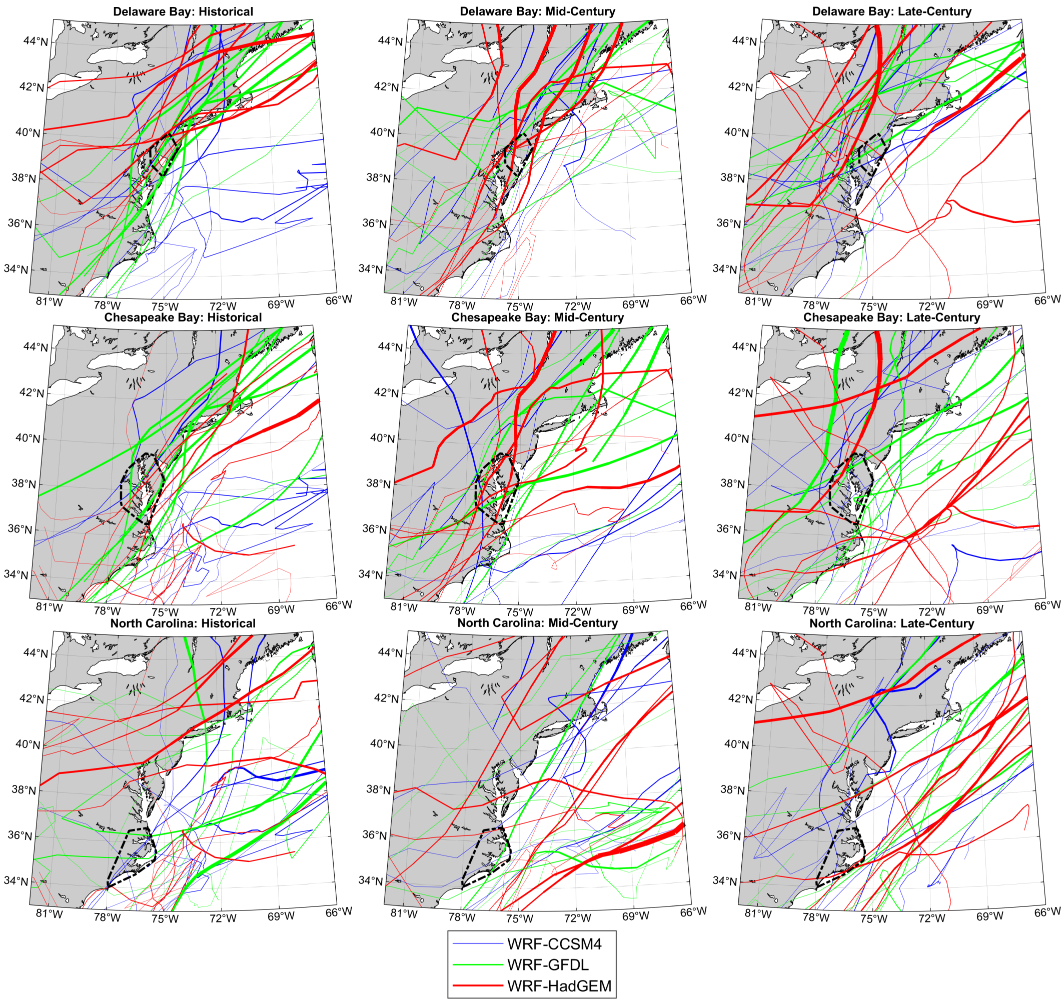

Figure 8. Same as Fig. 7 but for the southern subregions (top: Delaware Bay, middle: Chesapeake Bay, bottom: North Carolina).

WRF-CCSM4 produces no particularly strong storm tide generating ETCs affecting the southern subregions (Delaware Bay, Chesapeake Bay, and North Carolina) in any decade (Fig. 8). Regarding track patterns, there are generally more WRF-CCSM4 storm tracks passing through and just offshore of the North Carolina and the southern end of Chesapeake Bay in the historical decade than the future ones which could explain why future WRF-CCSM4 generated storm tides are moderately decreased (both the 3-season and 1-season PST) in these regions. WRF-GFDL produces a number of moderately intense storms directly impacting Delaware Bay and Chesapeake Bay in the historical decade. In future decades, WRF-GFDL storms are mostly less intense and there are fewer tracks that directly pass through or very close to the Delaware Bay and Chesapeake Bay subregions. However, WRF-GFDL storms tides are projected to be largely unchanged in these southern subregions with some small areas in Chesapeake Bay and North Carolina showing moderate increases. Noticeably, WRF-GFDL track angles in the historical decade are running very close to and parallel to the coastline while there is somewhat more variation in track angles for the future decades, which could be leading to certain tributaries of Chesapeake Bay having increased storm tides due to storm angles more favorable to surge. Furthermore, one may note the two moderately intense ETC tracks passing through the North Carolina subregion in the historical decade are in the west-to-east direction which would not be as favorable to surge in Albemarle and Pamlico Sounds as those tracks running just offshore of the subregion in the southwest-to-northeast direction plotted in the future decades. Compared to the historical decade, WRF-HadGEM storms affecting the Delaware Bay and Chesapeake Bay subregions are generally stronger and the track angle appears to be less oblique (more south-to-north running than parallel to the coast) in future decades. WRF-HadGEM generating storm tides in the northern areas Chesapeake Bay and Delaware Bay/River are indeed projected to increase in future decades while those in the areas exposed to the open ocean decrease. There also appear to be more intense WRF-HadGEM storms tracking just offshore, as well as a couple just inland, of the North Carolina subregion in the future decades. Indeed, WRF-HadGEM generated storm tides are mostly larger in the North Carolina subregion in future decades.

4 Discussion

4.1 Summary of Findings and Implications

Projected future changes in 1- and 3-season peak storm tide elevations along the NEC under the RCP8.5 climate change scenario were found to range between ± 0.3 m and ± 0.5 m, respectively. Variation due to RCM forcing is significant and generally greater than the variation between mid-century and late-century decades for the same RCM. In the New England and Long Island Sound subregions there is no general consensus on mid-century or late-century changes to PST. This is similar to the findings of Lin et al. (2019) who project a small increase to cool-season surge heights under CCSM4 GCM forcing and a decrease under GFDL GCM forcing at Boston, MA (located in the New England subregion) for the mid-to-late 21^{st} century (2054-2079). In particular, at Sussex County (#2) where Boston is located, our findings show little change to 1- and 3-season PSTs under WRF-CCSM4 forcing and a larger decrease under WRF-GFDL forcing. Furthermore, our findings are largely in agreement to Roberts et al. (2017); Lin et al. (2019) at New York County (#21) where we demonstrate little change to 1- and 3-season PST under WRF-HadGEM and WRF-CCSM4 forcing and a decrease under WRF-GFDL forcing. Roberts et al. (2017) focused on New York City and found no significant change to the cool-season maximum surge elevation, while Lin et al. (2019) show that 1-3 season return period surge heights at New York City were slightly increased under CCSM4 GCM forcing and decreased under GFDL GCM forcing.

While there is not perfect consensus on projected changes to PST in the New York/New Jersey Bight, Delaware Bay and Chesapeake Bay subregions, there is an indication that storm tides will increase at counties along the Hudson River, Delaware River and north-

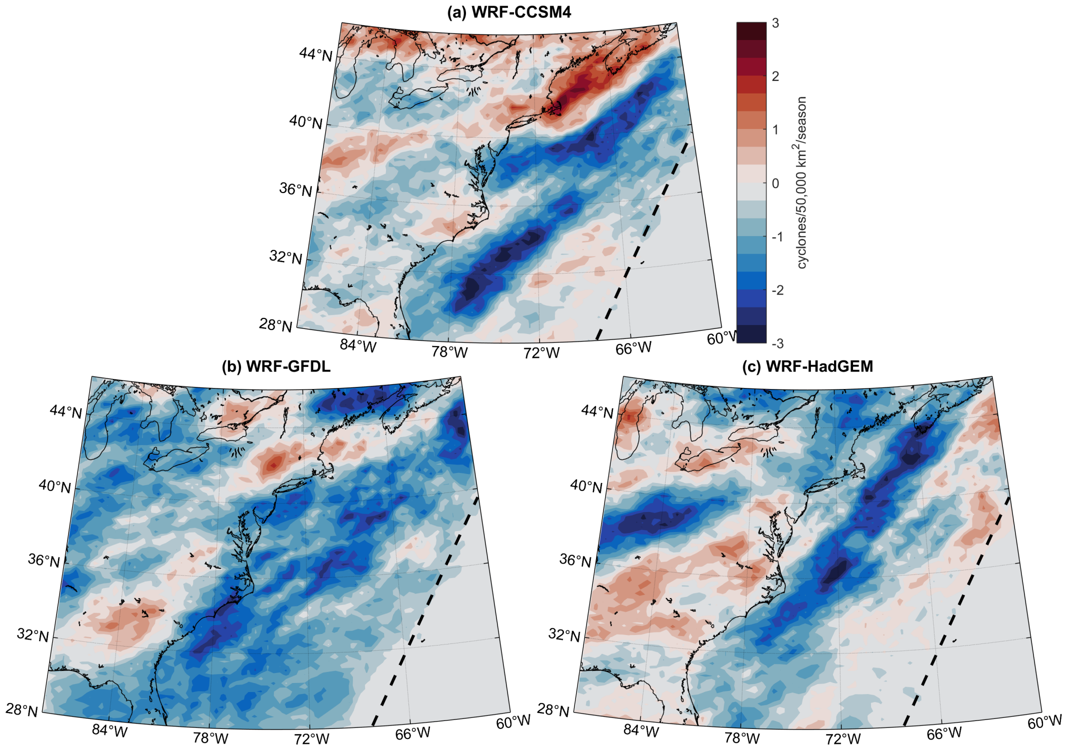

Figure 9. Cool-season cyclone density (number of cyclones per 50,000 km^2 per season) in the western North Atlantic Ocean during the late-century decade (2085-2094) as compared to the historical decade (1995-2004) for the regional climate model (RCM) simulations; (a) WRF-CCSM4, (b) WRF-GFDL, (c) WRF-HadGEM. Black dashed line indicates the edge of the RCM computational domains, explaining the null values here further offshore.

ern end of Chesapeake Bay, and decrease at counties facing the open ocean along the Mid-Atlantic Bight. This pattern is clearer for the late-century decade than the mid-century, and the magnitude of these changes varies fairly significantly between the RCMs. These findings are essentially the opposite to projected 10-yr surge height changes under CCSM4 and GFDL GCM forcing presented in Lin et al. (2019), where decreases were predicted in northern Chesapeake Bay and Delaware Bay and increases were predicted along the Mid-Atlantic Bight coast. However, in this study the strongest contrasting pattern of PST changes to the findings of Lin et al. (2019) were found under the WRF-HadGEM forcing (Lin et al. (2019) did not show results under HadGEM GCM forcing). We found that increased PST in the upper reaches of the large estuaries and rivers could be attributed to more intense ETCs that track just inland (to the northeast) of these subregions in a south-to-north direction, where southerly winds to the southeast of these ETC centers will be favorable to generating surge in these locations. However, in the historical period there appeared to be more ETCs tracking parallel to and just offshore of the coastline than in the future decades, likely resulting in the decreases to the PST for open coastal facing counties. To further that point, Fig. 9 illustrates a unanimous reduction in ETC density over most of the ocean offshore of the NEC in the late-century decade, a general finding that is also consistent with Colle et al. (2013); Zhang and Colle (2018).

There is little overall consensus on PST changes in the North Carolina subregion except for counties in the northern Albemarle Sound where the PST is projected to increase by all RCMs in both future decades. In these southern counties of the NEC region the tide-surge timing is not important, particularly in the Albemarle and Pamlico

Sounds in which the tidal amplitude is smaller than 10 cm. Instead, storm tides are driven by passing ETCs locally generating surge in the sounds. In contrast, the larger tidal range in the New England, Long Island Sound, New York/New Jersey Bight and Delaware Bay subregions leads to significant random uncertainty simply due to the phasing of the tides and weather conditions driving surge. In fact, the direction (increase or decrease) of projected changes to 1- and 3-season PST for each RCM forcing often depends on this random tide-surge timing in these subregions. Alternatively, the magnitude of change could be much greater than the tidal phase-based average especially for the 3-season PST.

The importance of the aforementioned projected changes to the PST depend on the relative comparisons to the magnitude and uncertainty of future SLR. Assuming that the GCMs provide a reasonable uncertainty range of future SLR under the RCP8.5 scenario (see Sect. 4.2), projected SLR is 0.2-0.8 m by mid-century and 0.4-1.3 m by late-century. This implies that projected SLR and PST changes are about equally as important to consider under the low-end of SLR projections for mid-century. By late-century, low-end SLR will be slightly more important to consider for coastal flooding potential than any storm climatology-driven PST changes. Under the high-end SLR projection, even by mid-century potential PST changes are 2-4 times smaller in magnitude, and by late-century PST changes are 3-6 times smaller in magnitude. Although this study, as well as others (Roberts et al., 2017; Lin et al., 2019), suggest that SLR will likely play a larger role in future changes to the cool-season coastal flooding potential in the 21^{st} century, we should consider the combination of SLR and PSTs taking into account the full range of possibilities based on random tide-surge timing.

4.2 Uncertainties and Limitations

The WRF-based dynamically downscaled RCM simulations were conducted over fairly short time periods (decadal) and a relatively small number of GCM members (three) were used. For this reason we avoided extrapolating our results to predict 100-year or other longer return periods using extreme value distributions. Furthermore, the RCM simulations were originally designed to investigate the North American continental climate and not particularly focused on resolving marine climatology. Thus, the atmospheric solution could potentially be partially influenced by the open boundary in the western North Atlantic Ocean. However, the RCM results were carefully bias-corrected and tested for boundary nudging effects. Future RCM simulations with greater computational resources will include larger portions of the ocean, more GCM members, and longer time periods.

On the hydrodynamic modeling side, the effects of wind-wave setup on coastal water elevations have been omitted in this study, primarily because wave modeling is significantly more computationally expensive than the hydrodynamic model. However, setup has been found to have a relatively small contribution to peak coastal water elevations in the NEC region (Marsooli & Lin, 2018), and is thus unlikely to impact our main finding. In addition, coastal flooding has been ignored, which if considered, generally results in lower water elevations on the ocean side compared to situations where inundation does not (or cannot) occur (Idier et al., 2019). Nevertheless, peak storm tide elevations recorded at the coast in our model simulations should generally be indicative of the coastal flooding potential.

We compared the magnitude of PST changes to SLR projections which we estimated from the parent GCMs for workflow self-consistency (avoiding external methodologies and models). It has been shown that CMIP5 GCMs may underestimate the externally driven anthropogenic component of SLR, particularly in the North Atlantic (Becker et al., 2016). Compared to probabilistic SLR scenarios computed for the 21^{st} century in the NEC region (Sweet et al., 2017), CCSM4/GFDL estimated SLR would indeed appear to correspond closest to the "low" scenario despite representing the RCP8.5 high-concentration pathway. However, HadGEM estimated SLR roughly corresponds to the "intermediate-high" scenario. We also note that storm tide dynamics and river discharge in the upper reaches of the estuaries and rivers may locally modulate SLR in a way that our analysis does not account for (Idier et al., 2019).

Data Availability

Datasets for this research are available without restriction at Pringle (2020) under the Creative Commons Attribution 4.0 International license. CCSM4 climate data was downloaded from `https://www.earthsystemgrid.org/`. GFDL-ESM2G and HadGEM2-ES climate data was downloaded from `https://esgf-node.llnl.gov/search/cmip5`. Specially, we chose the 'historical' experiment for the historical decade and the 'RCP8.5' experiment for the future decades, and the 'r1i1p1' ensemble for both experiments. Geospatial data describing the boundaries of United States counties used in our analysis was downloaded from `https://www.census.gov/geographies/mapping-files/time-series/geo/cartographic-boundary.html`.

Acknowledgments

WJP was supported by Laboratory Directed Research and Development (LDRD) Seed funding from Argonne National Laboratory, provided by the Director, Office of Science, of the U.S. Department of Energy under Contract No. DE-AC02-06CH11357. JW, KJR and VRK also acknowledge support from AT&T Services Inc. under a Strategic Partnership Project agreement A18131 to Argonne National Laboratory through U.S. Department of Energy contract DE-AC02-06CH11357. We acknowledge the National Energy Research Scientific Computing Center (NERSC), Argonne's Laboratory Computing Resource Center (LCRC), and the Argonne Leadership Computing Facility (ALCF) for providing the computational resources used to conduct the WRF modeling. Similarly, we thank LCRC for providing the computational resources used to conduct the ADCIRC modeling in this study. We are grateful to Dr. Emmanouil Flaounas for providing a modified form of the CycloTrack V2 code that we used to track cyclone central SLP.

References

Beardsley, R. C., Chen, C., & Xu, Q. (2013). Coastal flooding in Scituate (MA): A FVCOM study of the 27 December 2010 nor'easter. *Journal of Geophysical Research: Oceans*, *118*(11), 6030–6045. doi: 10.1002/2013JC008862

Becker, M., Karpytchev, M., Marcos, M., Jevrejeva, S., & Lennartz-Sassinek, S. (2016). Do climate models reproduce complexity of observed sea level changes? *Geophysical Research Letters*, *43*(10), 5176–5184. doi: 10.1002/2016GL068971

Booth, J. F., Naud, C. M., & Willison, J. (2018). Evaluation of extratropical cyclone precipitation in the North Atlantic basin: An analysis of ERA-Interim, WRF, and two CMIP5 models. *Journal of Climate*, *31*(6), 2345–2360. doi: 10.1175/JCLI-D-17-0308.1

Booth, J. F., Rieder, H. E., & Kushnir, Y. (2016). Comparing hurricane and extratropical storm surge for the Mid-Atlantic and Northeast Coast of the United States for 1979-2013. *Environmental Research Letters*, *11*(9). doi: 10.1088/1748-9326/11/9/094004

Bunya, S., Dietrich, J. C., Westerink, J. J., Ebersole, B. A., Smith, J. M., Atkinson, J. H., ... Roberts, H. J. (2010, feb). A High-Resolution Coupled Riverine Flow, Tide, Wind, Wind Wave, and Storm Surge Model for Southern Louisiana and Mississippi. Part I: Model Development and Validation. *Monthly Weather Review*, *138*(2), 345–377. Retrieved from `http://journals.ametsoc.org/doi/abs/10.1175/2009MWR2906.1` doi: 10.1175/2009MWR2906.1

Catalano, A. J., & Broccoli, A. J. (2018). Synoptic characteristics of surgeproducing extratropical cyclones along the northeast coast of the United States. *Journal of Applied Meteorology and Climatology*, *57*(1), 171–184. doi: 10.1175/JAMC-D-17-0123.1

Chang, E. K. (2013). CMIP5 projection of significant reduction in extratropical cyclone activity over North America. *Journal of Climate*, *26*(24), 9903–9922. doi: 10.1175/JCLI-D-13-00209.1

Colle, B. A., Buonauto, F., Bowman, M. J., Wilson, R. E., Flood, R., Hunter, R., ... Hill, D. (2008). New York City's Vulnerability to Coastal Flooding: Storm Surge Modeling of Past Cyclones. *Bulletin of the American Meteorological Society*, *89*, 829–841. doi: 10.1175/2007BAMS2401.1

Colle, B. A., Rojowsky, K., & Buonaito, F. (2010). New York city storm surges: Climatology and an analysis of the wind and cyclone evolution. *Journal of Applied Meteorology and Climatology*, *49*(1), 85–100. doi: 10.1175/2009JAMC2189.1

Colle, B. A., Zhang, Z., Lombardo, K. A., Chang, E., Liu, P., & Zhang, M. (2013). Historical evaluation and future prediction of eastern North American and Western Atlantic extratropical cyclones in the CMIP5 models during the cool season. *Journal of Climate*, *26*(18), 6882–6903. doi: 10.1175/JCLI-D-12-00498.1

Egbert, G. D., & Erofeeva, S. Y. (2019). *TPXO9-Atlas.* Retrieved from `http://volkov.oce.orst.edu/tides/tpxo9{\_}atlas.html`

European Centre for Medium-Range Weather Forecasts. (2019). *ERA5 Reanalysis (0.25 Degree Latitude-Longitude Grid).* Boulder, CO: Research Data Archive at the National Center for Atmospheric Research, Computational and Information Systems Laboratory. Retrieved from `https://doi.org/10.5065/BH6N-5N20` doi: 10.5065/BH6N-5N20

Flaounas, E., Kotroni, V., Lagouvardos, K., & Flaounas, I. (2014). CycloTRACK (v1.0)-tracking winter extratropical cyclones based on relative vorticity: Sensitivity to data filtering and other relevant parameters. *Geoscientific Model Development*, *7*(4), 1841–1853. doi: 10.5194/gmd-7-1841-2014

Hope, M. E., Westerink, J. J., Kennedy, A. B., Kerr, P. C., Dietrich, J. C., Dawson, C., ... Westerink, L. G. (2013, sep). Hindcast and validation of Hurricane Ike (2008) waves, forerunner, and storm surge. *Journal of Geophysical Research: Oceans*, *118*(9), 4424–4460. Retrieved from `http://doi.wiley.com/10.1002/jgrc.20314` doi: 10.1002/jgrc.20314

Horsburgh, K. J., & Wilson, C. (2007). Tide-surge interaction and its role in the distribution of surge residuals in the North Sea. *Journal of Geophysical Research: Oceans*, *112*(8), 1–13. doi: 10.1029/2006JC004033

Idier, D., Bertin, X., Thompson, P., & Pickering, M. D. (2019). Interactions Between Mean Sea Level, Tide, Surge, Waves and Flooding: Mechanisms and Contributions to Sea Level Variations at the Coast. *Surveys in Geophysics*, *40*(6), 1603–1630. Retrieved from `https://doi.org/10.1007/s10712-019-09549-5` doi: 10.1007/s10712-019-09549-5

Lin, N., Marsooli, R., & Colle, B. A. (2019). Storm surge return levels induced by mid-to-late-twenty-first-century extratropical cyclones in the Northeastern United States. *Climatic Change*, *154*(1-2), 143–158. doi: 10.1007/s10584-019-02431-8

Long, Z., Perrie, W., Gyakum, J., Laprise, R., & Caya, D. (2009). Scenario changes in the climatology of winter midlatitude cyclone activity over eastern North America and the Northwest Atlantic. *Journal of Geophysical Research Atmospheres*, *114*(12), 1–13. doi: 10.1029/2008JD010869

Luettich, R. A., & Westerink, J. J. (2004). *Formulation and Numerical Implementation of the 2D/3D ADCIRC Finite Element Model Version 44.XX* (Tech. Rep.). University of North Carolina at Chapel Hill & University of Notre Dame.

Marsooli, R., & Lin, N. (2018). Numerical Modeling of Historical Storm Tides and Waves and Their Interactions Along the U.S. East and Gulf Coasts. *Journal of Geophysical Research: Oceans*, *123*(5), 3844–3874. doi: 10.1029/2017JC013434

Marsooli, R., Lin, N., Emanuel, K., & Feng, K. (2019). Climate change exacerbates hurricane flood hazards along U.S. Atlantic coast in spatially varying patterns. *Nature Communications*, *10*, 3785. Retrieved from `http://dx.doi.org/10.1038/s41467-019-11755-z` doi: 10.1038/s41467-019-11755-z

Parker, B. B. (2007). *Tidal analysis and prediction.* Silver Spring, MD.

Pringle, W. J. (2020). *Projected Changes to Cool-Season Storm Tides along the Northeastern U.S. Coast: Dataset.* Zenodo. doi: 10.5281/zenodo.4320052

Pringle, W. J., & Roberts, K. J. (2020). *CHLNDDEV/OceanMesh2D: OceanMesh2D V3.0.0.* Zenodo. doi: 10.5281/zenodo.3721137

Pringle, W. J., Wirasaet, D., Roberts, K. J., & Westerink, J. (2020). Global Storm Tide Modeling with ADCIRC v55: Unstructured Mesh Design and Performance. *Geoscientific Model Development Discussions*, in review. doi: 10.5194/gmd-2020-123

Riahi, K., Rao, S., Krey, V., Cho, C., Chirkov, V., Fischer, G., ... Rafaj, P. (2011). RCP 8.5-A scenario of comparatively high greenhouse gas emissions. *Climatic Change*, *109*(1), 33–57. doi: 10.1007/s10584-011-0149-y

Roberts, K. J. (2015). *An Application of Regression for Storm Surge Prediction along the New York/New Jersey Coast in Climate Models* (Masters Thesis, Stony Brook University). Retrieved from `http://hdl.handle.net/11401/76207`

Roberts, K. J., Colle, B. A., & Korfe, N. (2017). Impact of simulated twenty-first-century changes in extratropical cyclones on coastal flooding at the Battery, New York City. *Journal of Applied Meteorology and Climatology*, *56*(2), 415–432. doi: 10.1175/JAMC-D-16-0088.1

Roberts, K. J., Pringle, W. J., & Westerink, J. J. (2019). OceanMesh2D 1.0: MATLAB-based software for two-dimensional unstructured mesh generation in coastal ocean modeling. *Geoscientific Model Development*, *12*, 1847–1868. doi: 10.5194/gmd-12-1847-2019

Roberts, K. J., Pringle, W. J., Westerink, J. J., Contreras, M. T., & Wirasaet, D. (2019). On the automatic and a priori design of unstructured mesh resolution for coastal ocean circulation models. *Ocean Modelling*, *144*, 101509. doi: 10.1016/j.ocemod.2019.101509

Schwalm, C. R., Glendon, S., & Duffy, P. B. (2020). RCP8.5 tracks cumulative CO2 emissions. *Proceedings of the National Academy of Sciences*, *117*(33), 19656–19657. doi: 10.1073/pnas.2007117117

Seiler, C., Zwiers, F. W., Hodges, K. I., & Scinocca, J. F. (2018). How does dynamical downscaling affect model biases and future projections of explosive extratropical cyclones along North America's Atlantic coast? *Climate Dynamics*, *50*(1-2), 677–692. doi: 10.1007/s00382-017-3634-9

Sherwood, S. C., Bony, S., & Dufresne, J. L. (2014). Spread in model climate sensitivity traced to atmospheric convective mixing. *Nature*, *505*(7481), 37–42. doi: 10.1038/nature12829

Sweet, W. V., Kopp, R. E., Weaver, C. P., Obeysekera, J., Horton, R. M., Thieler, E. R., & Zervas, C. (2017). *Global and Regional Sea Level Rise Scenarios for the United States* (Tech. Rep. No. NOS CO-OPS 083). NOAA/NOS Center for Operational Oceanographic Products and Services. Retrieved from `https://tidesandcurrents.noaa.gov/publications/techrpt83{\_}Global{\_}and{\_}Regional{\_}SLR{\_}Scenarios{\_}for{\_}the{\_}US{\_}final.pdf`

Taylor, K. E., Stouffer, R. J., & Meehl, G. A. (2012). An overview of CMIP5 and the experiment design. *Bulletin of the American Meteorological Society*, *93*(4), 485–498. doi: 10.1175/BAMS-D-11-00094.1

Teng, H., Washington, W. M., & Meehl, G. A. (2008). Interannual variations and future change of wintertime extratropical cyclone activity over North America in CCSM3. *Climate Dynamics*, *30*(7-8), 673–686. doi: 10.1007/s00382-007-0314-1

Tozer, B., Sandwell, D. T., Smith, W. H., Olson, C., Beale, J. R., & Wessel, P. (2019). Global Bathymetry and Topography at 15 Arc Sec: SRTM15+. *Earth and Space Science*, *6*(10), 1847–1864. doi: 10.1029/2019EA000658

Wang, J., & Kotamarthi, V. R. (2015). High-resolution dynamically downscaled projections of precipitation in the mid and late 21st century over North America. *Earth's Future*, *3*(7), 268–288. doi: 10.1002/2015EF000304

Westerink, J. J., Luettich, R. A., Feyen, J. C., Atkinson, J. H., Dawson, C., Roberts, H. J., ... Pourtaheri, H. (2008, mar). A Basin- to Channel-Scale Unstructured Grid Hurricane Storm Surge Model Applied to Southern Louisiana. *Monthly Weather Review*, *136*(3), 833–864. Retrieved from `http://journals.ametsoc.org/doi/abs/10.1175/2007MWR1946.1` doi: 10.1175/2007MWR1946.1

Zhang, Z., & Colle, B. A. (2018). Impact of dynamically downscaling two CMIP5 models on the historical and future changes in winter extratropical cyclones along the East Coast of North America. *Journal of Climate*, *31*(20), 8499–8525. doi: 10.1175/JCLI-D-18-0178.1

Zobel, Z., Wang, J., Wuebbles, D. J., & Kotamarthi, V. R. (2018). Evaluations of high-resolution dynamically downscaled ensembles over the contiguous United States. *Climate Dynamics*, *50*(3-4), 863–884. doi: 10.1007/s00382-017-3645-6

Figure 1.

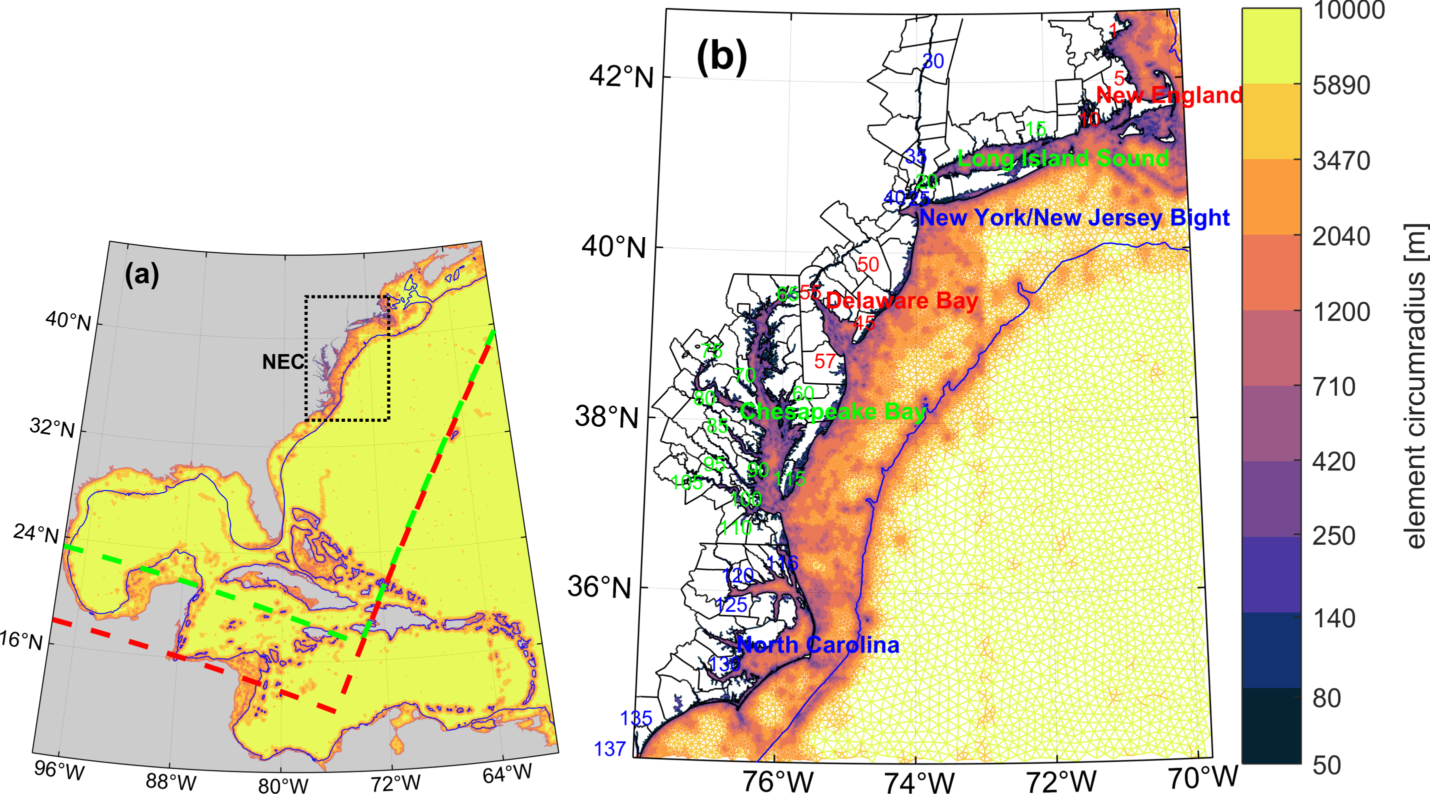
(a)
NEC
40°N
32°N
24°N
16°N
96°W
88°W
80°W
72°W
64°W
(b)
42°N
40°N
38°N
36°N
76°W
74°W
72°W
70°W
New England
Long Island Sound
New York/New Jersey Bight
Delaware Bay
Chesapeake Bay
North Carolina
1
5
10
15
20
25
30
35
40
45
50
55
57
60
65
70
75
80
85
90
95
100
105
110
115
116
120
125
130
135
137
10000
5890
3470
2040
1200
710
420
250
140
80
50
element circumradius [m]

Figure 2.

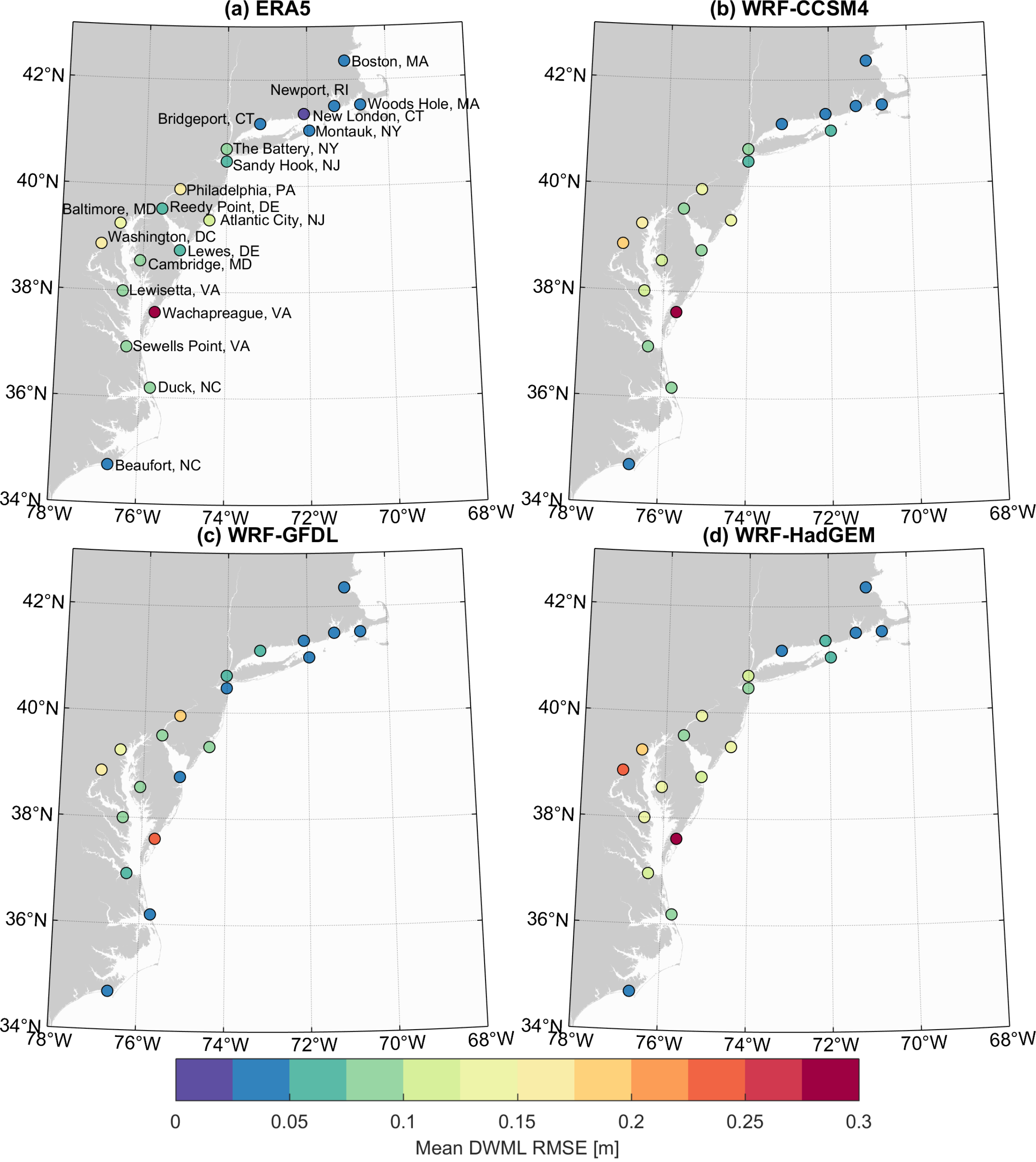

(a) ERA5
(b) WRF-CCSM4
(c) WRF-GFDL
(d) WRF-HadGEM
Boston, MA
Newport, RI
Woods Hole, MA
Bridgeport, CT
New London, CT
Montauk, NY
The Battery, NY
Sandy Hook, NJ
Philadelphia, PA
Baltimore, MD
Reedy Point, DE
Atlantic City, NJ
Washington, DC
Lewes, DE
Cambridge, MD
Lewisetta, VA
Wachapreague, VA
Sewells Point, VA
Duck, NC
Beaufort, NC
42°N
40°N
38°N
36°N
34°N
78°W
76°W
74°W
72°W
70°W
68°W
0
0.05
0.1
0.15
0.2
0.25
0.3
Mean DWML RMSE [m]

Figure 3.

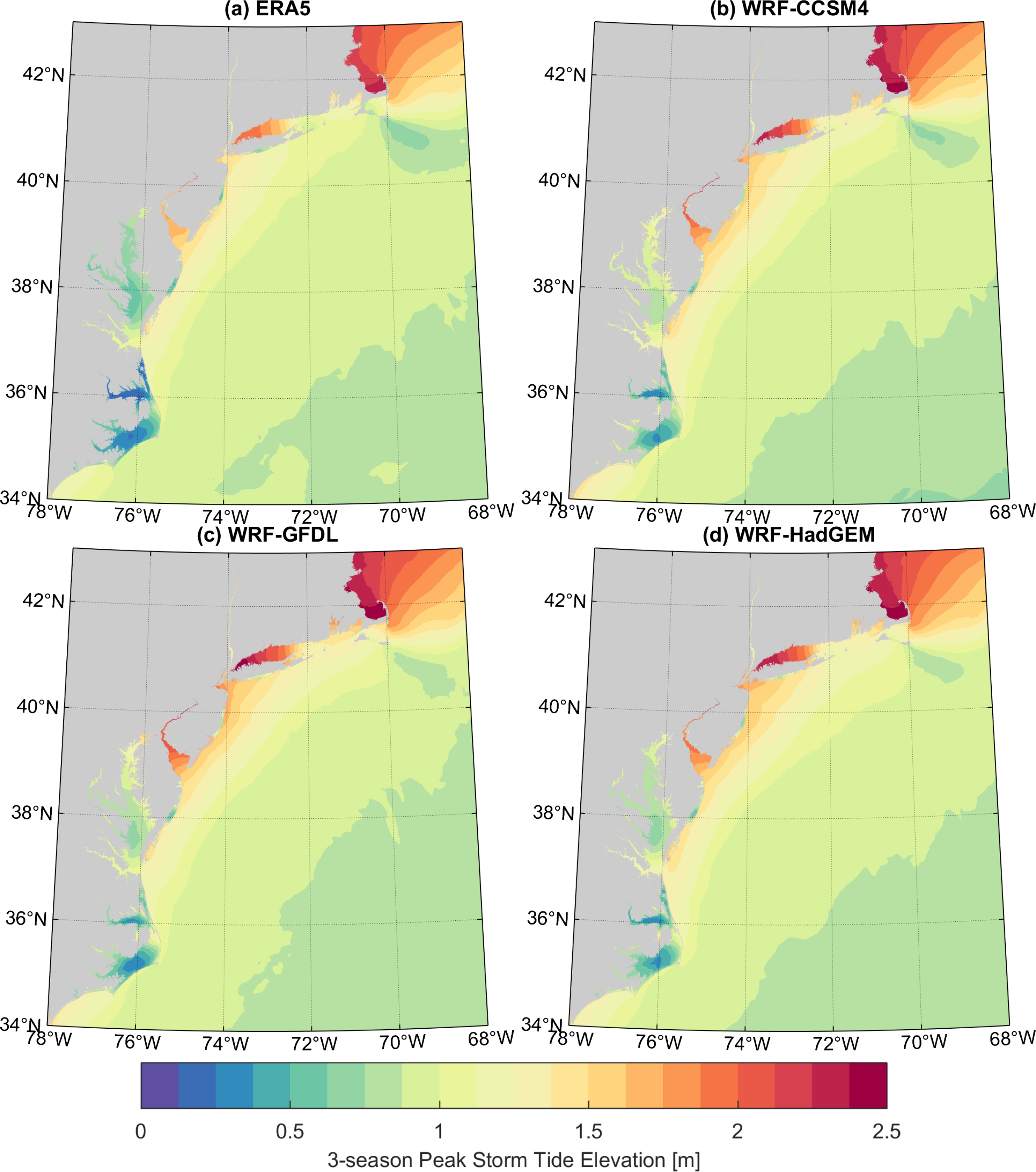

(a) ERA5
(b) WRF-CCSM4
(c) WRF-GFDL
(d) WRF-HadGEM
42°N
40°N
38°N
36°N
34°N
78°W
76°W
74°W
72°W
70°W
68°W
0
0.5
1
1.5
2
2.5
3-season Peak Storm Tide Elevation [m]

Figure 4.

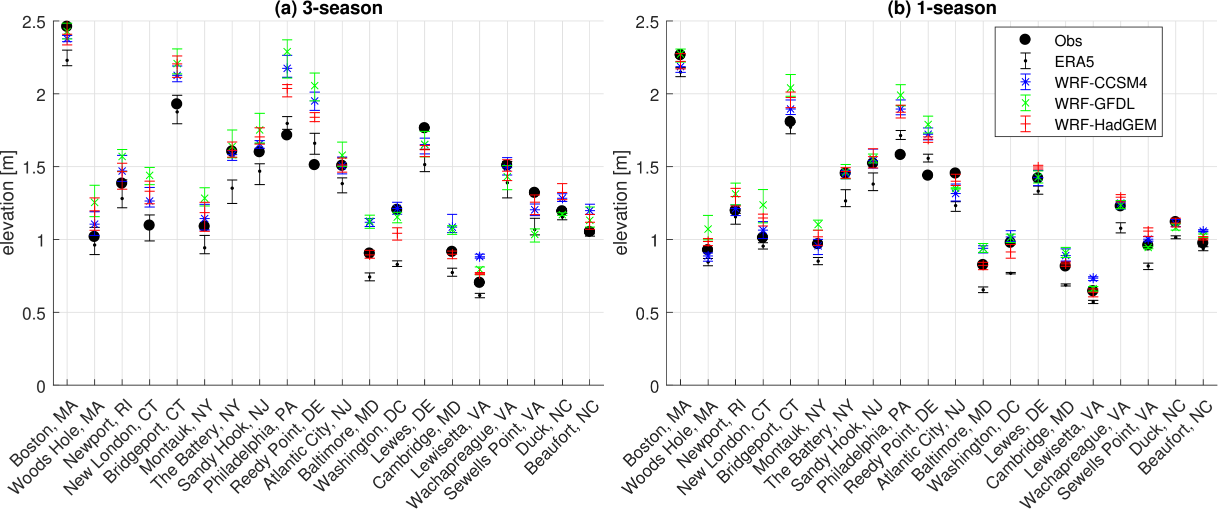
(a) 3-season
(b) 1-season
elevation [m]
Obs
ERA5
WRF-CCSM4
WRF-GFDL
WRF-HadGEM
Boston, MA
Woods Hole, MA
Newport, RI
New London, CT
Bridgeport, CT
Montauk, NY
The Battery, NY
Sandy Hook, NJ
Philadelphia, PA
Reedy Point, DE
Atlantic City, NJ
Baltimore, MD
Washington, DC
Lewes, DE
Cambridge, MD
Lewisetta, VA
Wachapreague, VA
Sewells Point, VA
Duck, NC
Beaufort, NC

Figure 5.

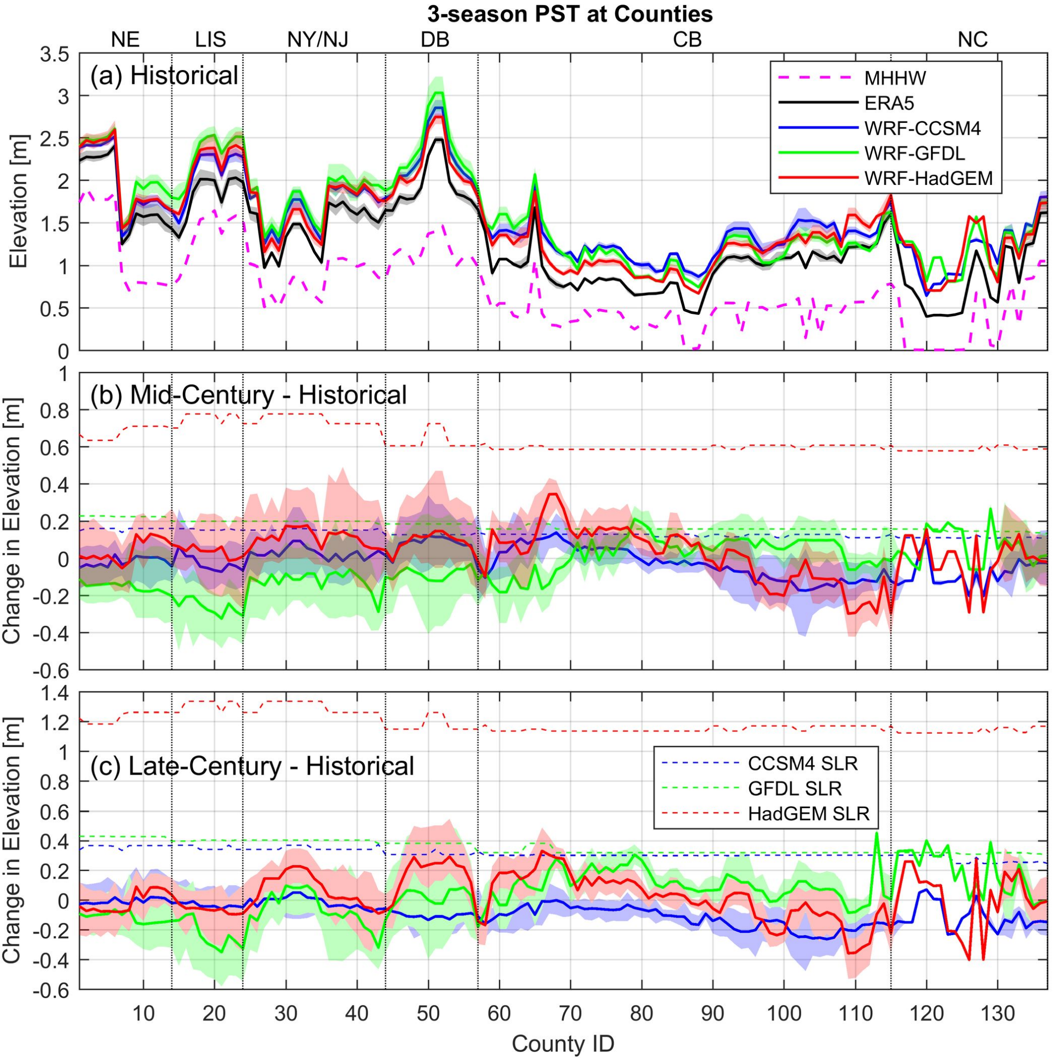

3-season PST at Counties
NE
LIS
NY/NJ
DB
CB
NC
(a) Historical
MHHW
ERA5
WRF-CCSM4
WRF-GFDL
WRF-HadGEM
Elevation [m]
(b) Mid-Century - Historical
Change in Elevation [m]
(c) Late-Century - Historical
CCSM4 SLR
GFDL SLR
HadGEM SLR
Change in Elevation [m]
County ID

Figure 6.

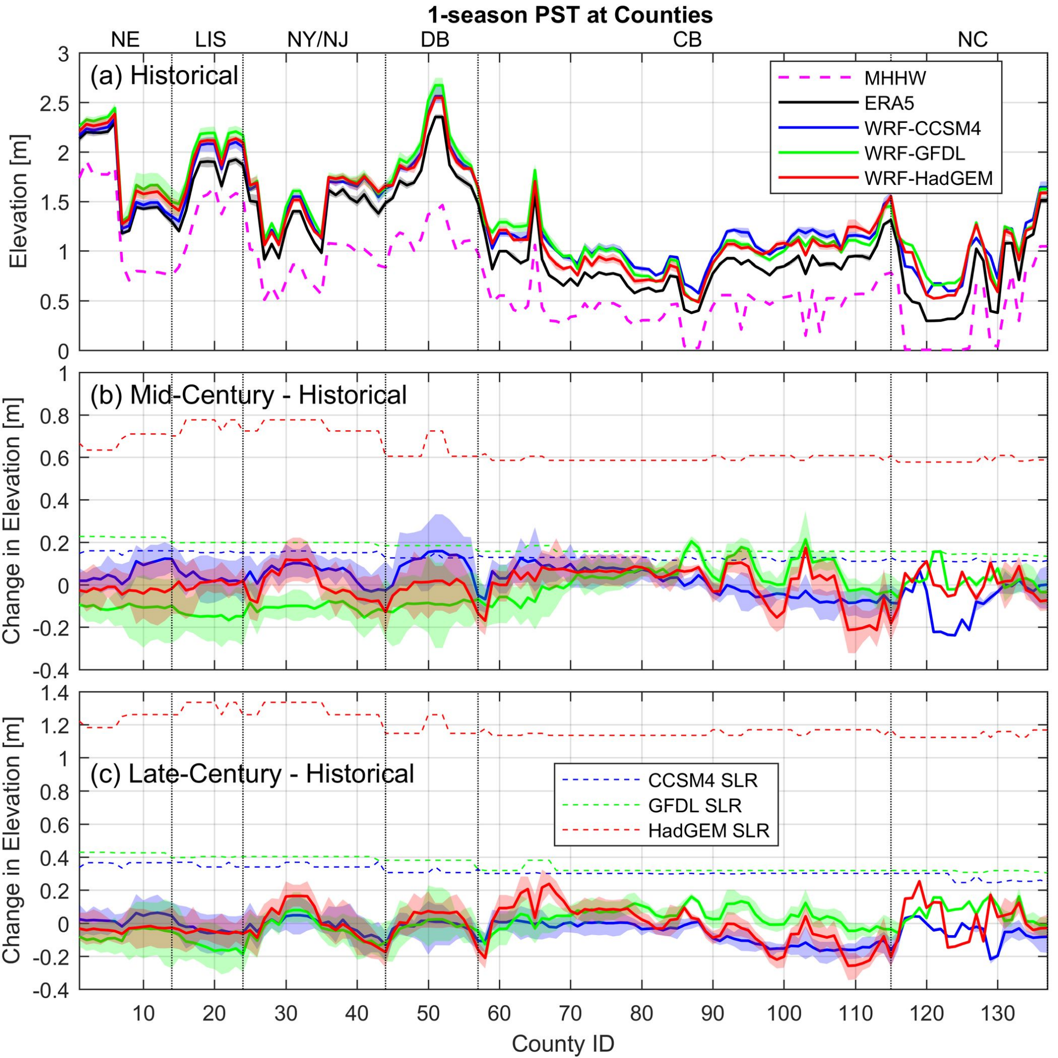
1-season PST at Counties
NE
LIS
NY/NJ
DB
CB
NC
(a) Historical
MHHW
ERA5
WRF-CCSM4
WRF-GFDL
WRF-HadGEM
Elevation [m]
(b) Mid-Century - Historical
Change in Elevation [m]
(c) Late-Century - Historical
CCSM4 SLR
GFDL SLR
HadGEM SLR
County ID

Figure 7.

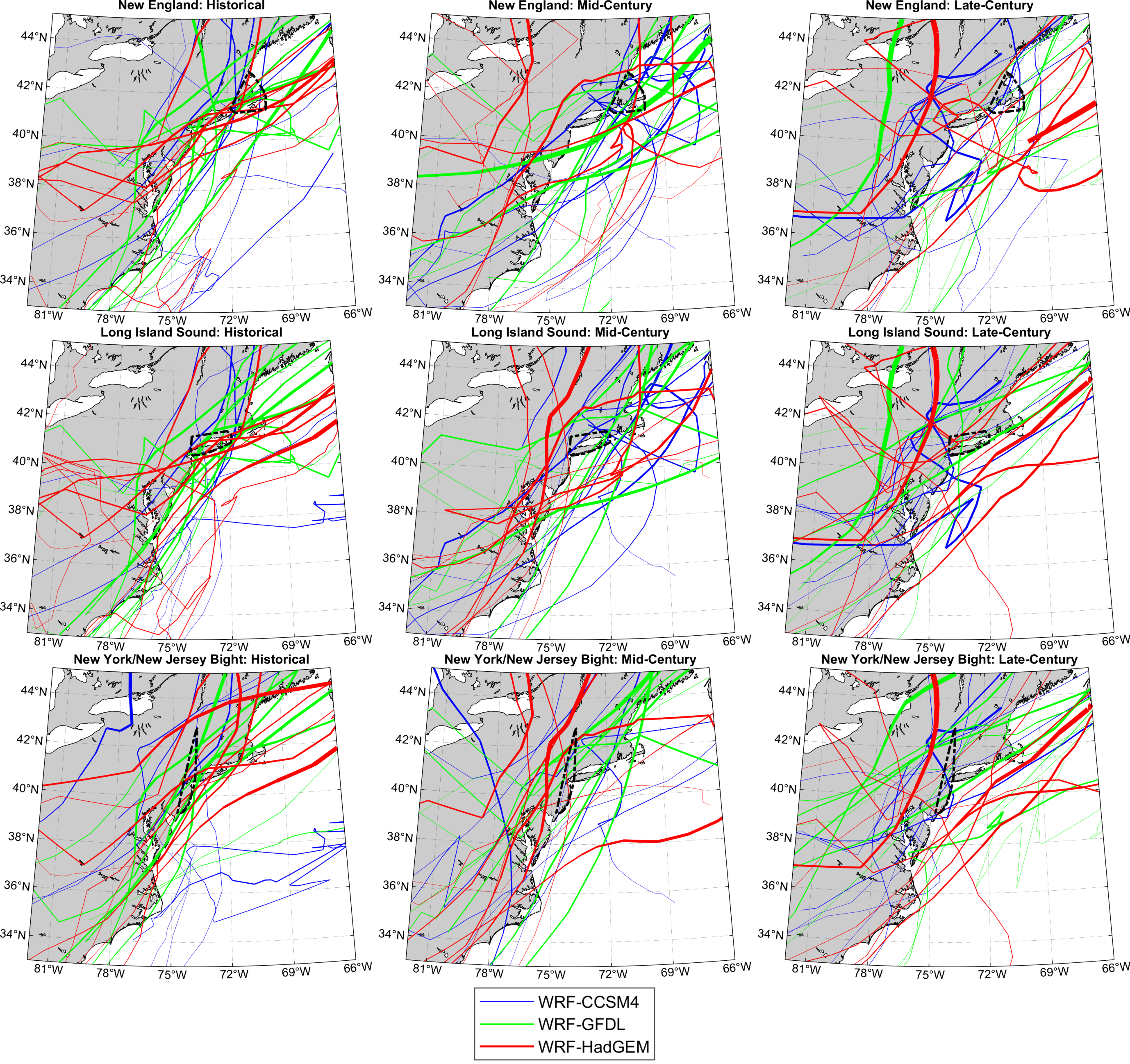

New England: Historical
New England: Mid-Century
New England: Late-Century
Long Island Sound: Historical
Long Island Sound: Mid-Century
Long Island Sound: Late-Century
New York/New Jersey Bight: Historical
New York/New Jersey Bight: Mid-Century
New York/New Jersey Bight: Late-Century
44°N
42°N
40°N
38°N
36°N
34°N
81°W
78°W
75°W
72°W
69°W
66°W
WRF-CCSM4
WRF-GFDL
WRF-HadGEM

Figure 8.

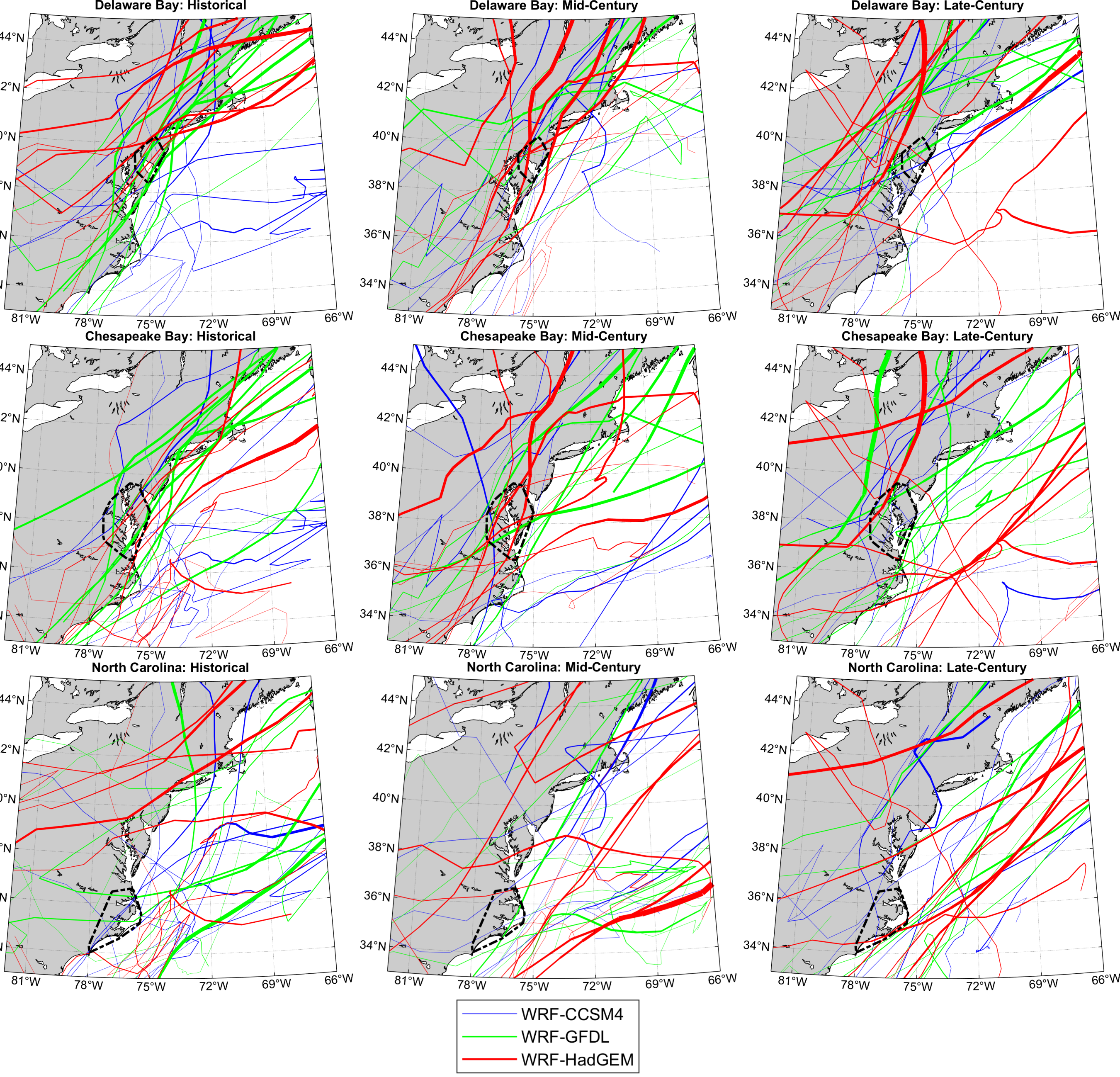
Delaware Bay: Historical
Delaware Bay: Mid-Century
Delaware Bay: Late-Century
Chesapeake Bay: Historical
Chesapeake Bay: Mid-Century
Chesapeake Bay: Late-Century
North Carolina: Historical
North Carolina: Mid-Century
North Carolina: Late-Century
44°N
42°N
40°N
38°N
36°N
34°N
81°W
78°W
75°W
72°W
69°W
66°W
WRF-CCSM4
WRF-GFDL
WRF-HadGEM

Figure 9.

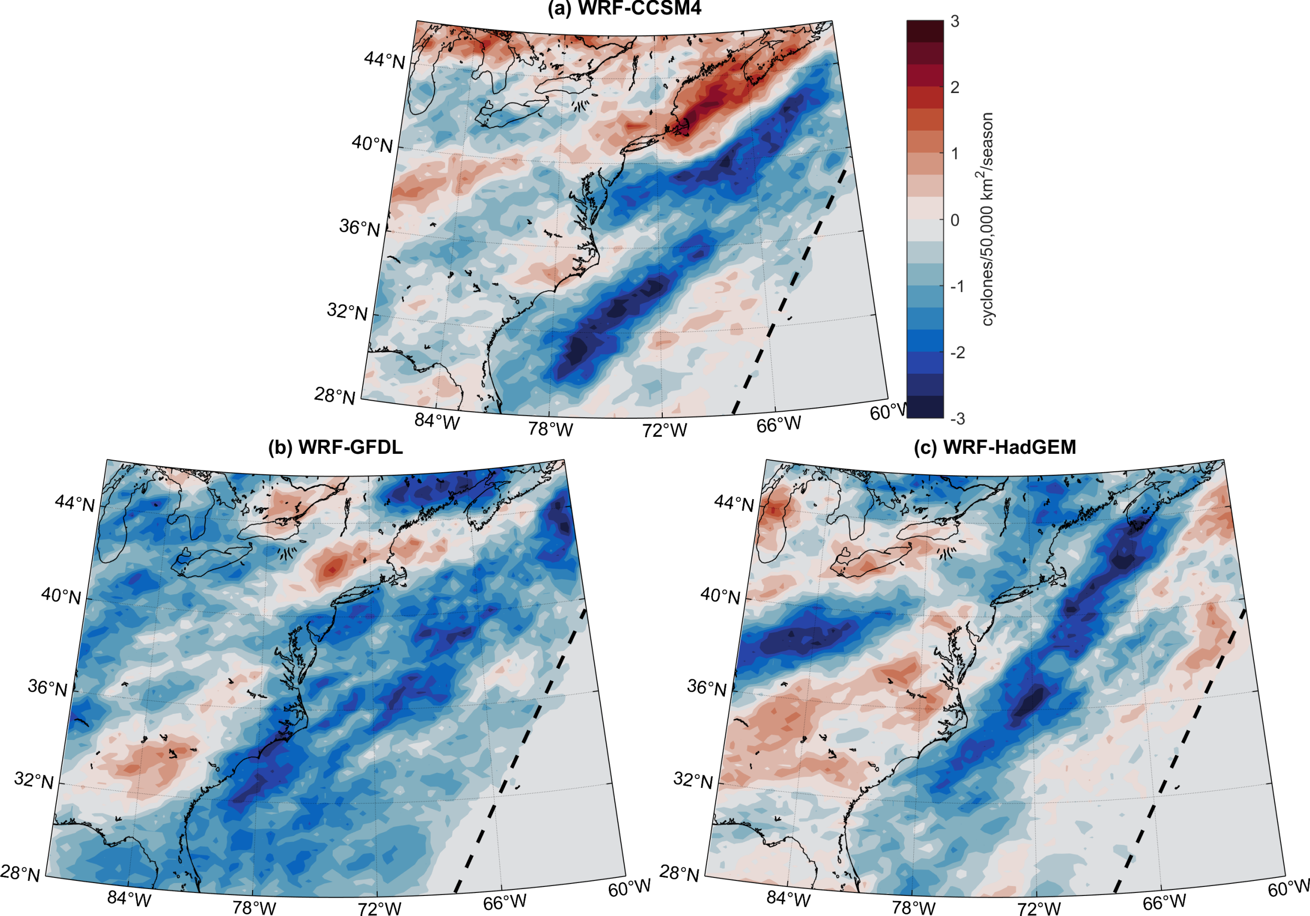

(a) WRF-CCSM4
(b) WRF-GFDL
(c) WRF-HadGEM
cyclones/50,000 km^2/season
3
2
1
0
-1
-2
-3
44°N
40°N
36°N
32°N
28°N
84°W
78°W
72°W
66°W
60°W

Supporting Information for "Projected Changes to Cool-Season Storm Tides in the 21st Century along the Northeastern United States Coast"

William J. Pringle[1], Jiali Wang[1], Keith J. Roberts[2], Veerabhadra R. Kotamarthi[1]

[1]Environmental Science Division, Argonne National Laboratory, Lemont, IL, USA

[2]School of Marine and Atmospheric Science, Stony Brook University, NY, USA

Contents of this file

1. Figures S1 to S7

Introduction This supplementary contains figures that summarizes the accuracy of low-level winds and extratropical cyclone (ETC) characteristics of the 12-km horizontal resolution downscaled regional climate models (RCMs; computational domain shown in Fig. S1) in the northeastern United States coast (NEC) region during the historical cool-season (November-March) decade (1995-2004).

RCM-simulated near-surface wind velocities (10-m above ground) are compared with National Buoy Data Center (NBDC) offshore buoy observations in Figs. S2-S5. Observed winds at the NBDC anemometers are adjusted to 10-m above ground height through the Power-law method (Hsu et al., 1994). Since the WRF-based RCM simulations are not a reanalysis (i.e., the date of occurrence is meaningless), the root-mean-square-error

(RMSE) of wind speeds shown in Fig. S2 is computed on the quantile-quantile plot distribution.

Figures S6-S7 show the density and intensity distributions, respectively, of ETCs represented by the RCMs as compared to 0.25° ERA5 reanalysis data (European Centre for Medium-Range Weather Forecasts, 2019). Individual cyclones are extracted from the meteorological data by tracking the local minimums of sea level pressure (SLP) using Version 2 of CycloneTrack (Flaounas et al., 2014), a cyclone tracking algorithm. To filter out small scales in SLP a 2-D Gaussian smoothing kernel with a standard deviation of 10 is used. The ERA5 reanalysis data was sampled at 3-hourly intervals to match the RCM model outputs.

References

European Centre for Medium-Range Weather Forecasts. (2019). *ERA5 Reanalysis (0.25 Degree Latitude-Longitude Grid).* Boulder, CO: Research Data Archive at the National Center for Atmospheric Research, Computational and Information Systems Laboratory. Retrieved from `https://doi.org/10.5065/BH6N-5N20` doi: 10.5065/BH6N-5N20

Flaounas, E., Kotroni, V., Lagouvardos, K., & Flaounas, I. (2014). CycloTRACK (v1.0)-tracking winter extratropical cyclones based on relative vorticity: Sensitivity to data filtering and other relevant parameters. *Geoscientific Model Development*, *7*(4), 1841–1853. doi: 10.5194/gmd-7-1841-2014

Hsu, S. A., Meindl, E. A., & Gilhousen, D. B. (1994). Determining the Power-Law Wind-Profile Exponent under Near-Neutral Stability Conditions at Sea. *Journal of Applied Meteorology and Climatology*, *33*(6), 757–765. doi: 10.1175/1520-0450(1994)

033⟨0757:DTPLWP⟩2.0.CO;2

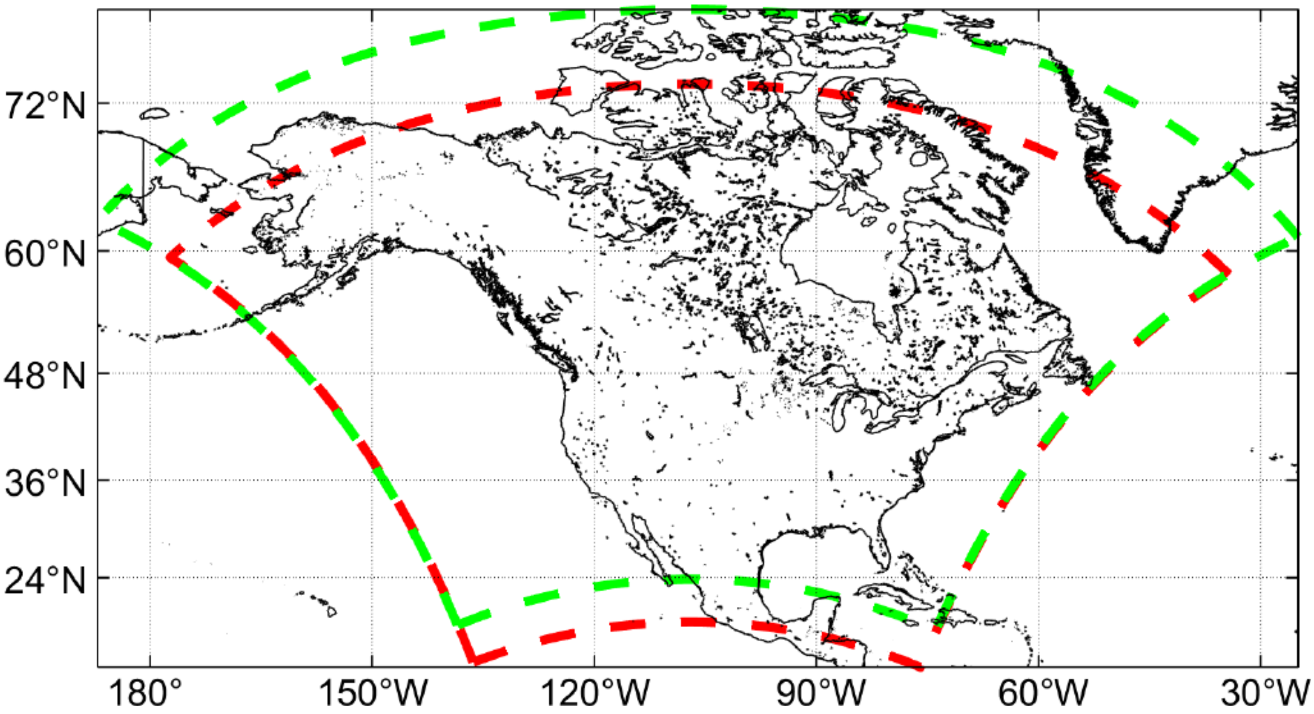

Figure S1. Computational domain (dashed regions) of the three WRF-based RCMs (WRF-CCSM4: green, WRF-GFDL/HadGEM: red).

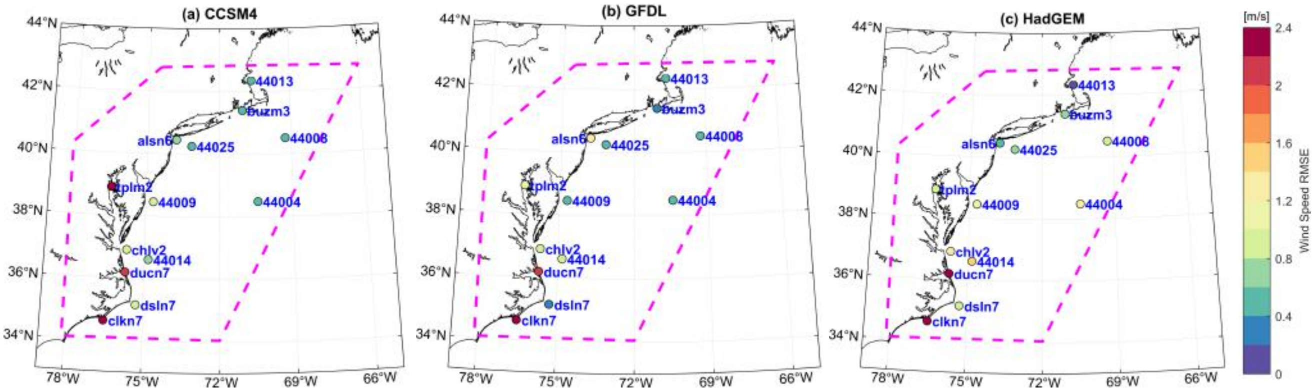

Figure S2. Accuracy (RMSE) of simulated 10-m wind speeds during the cool-season at NDBC buoys in the NEC region for the historical decade (1995-2004) by the three WRF-based RCMs; (a) WRF-CCSM4, (b) WRF-GFDL, (c) WRF-HadGEM.

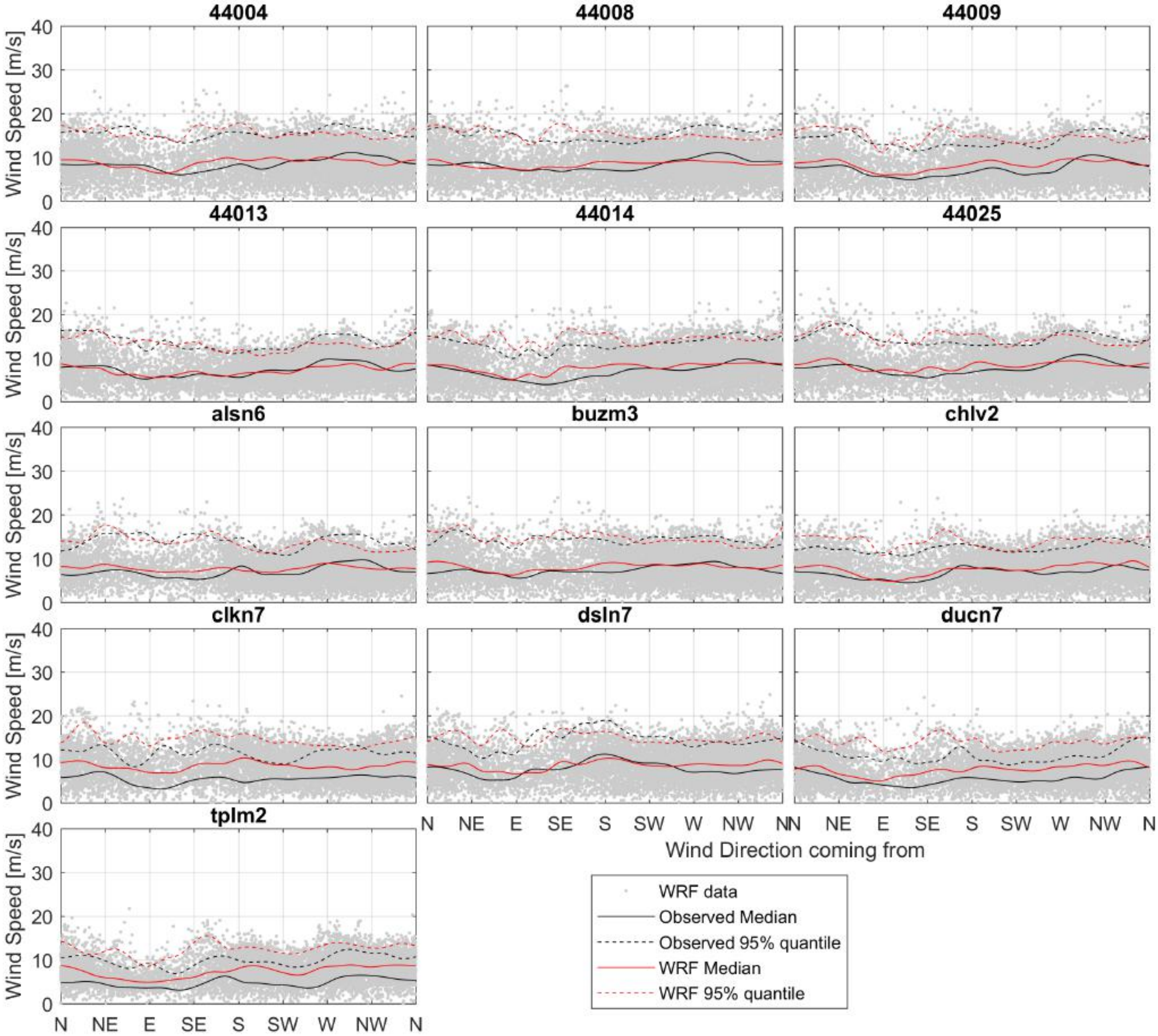

Figure S3. Distribution of WRF-CCSM4 simulated wind speeds and directions at NDBC buoys in the NEC region for the historical decade (1995-2004). Comparisons are shown against the median and 95% quantile of measured wind speeds at the NDBC buoys whose locations are shown in Fig. S2.

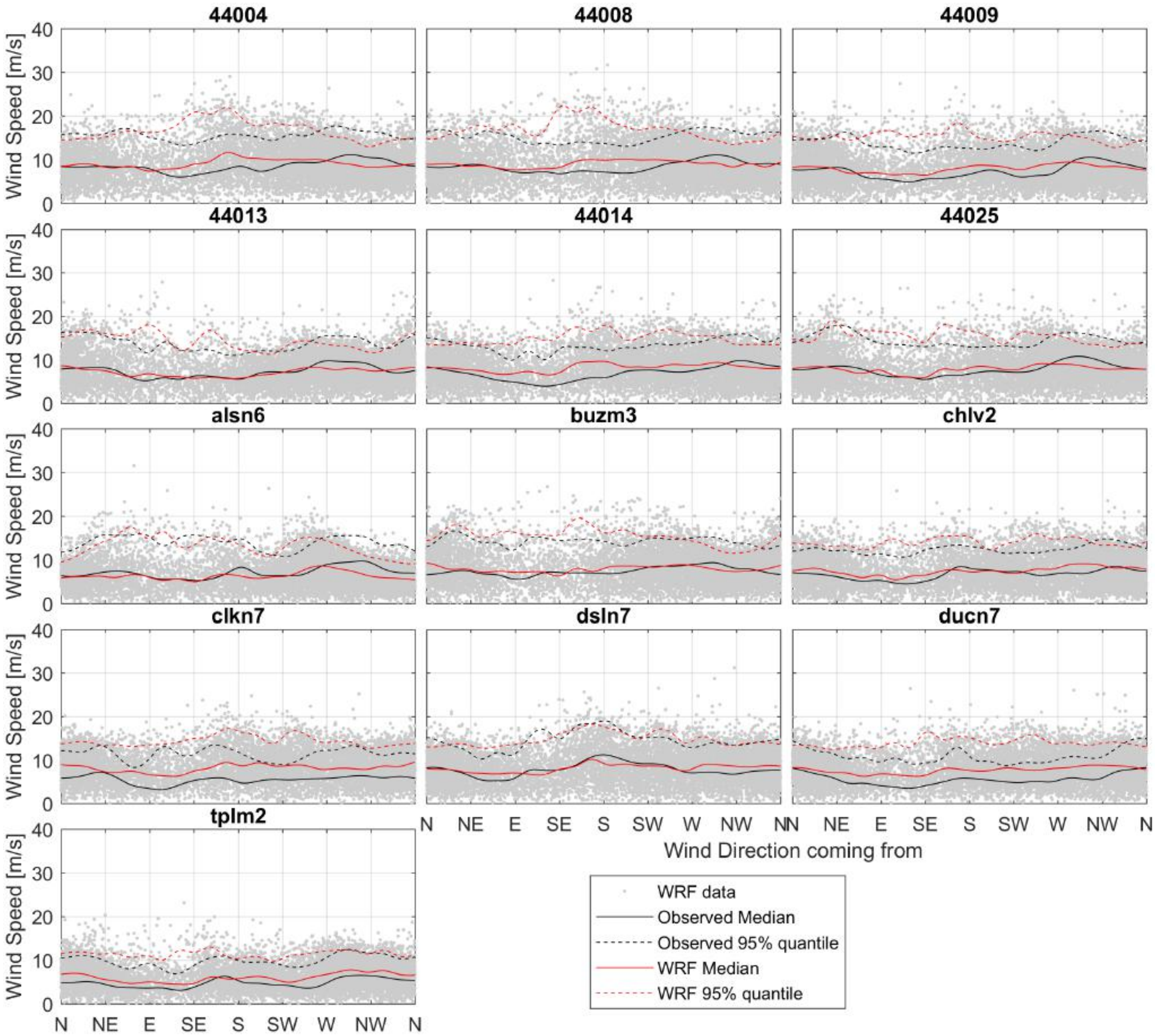

Figure S4. Same as Fig. S3 but for WRF-GFDL.

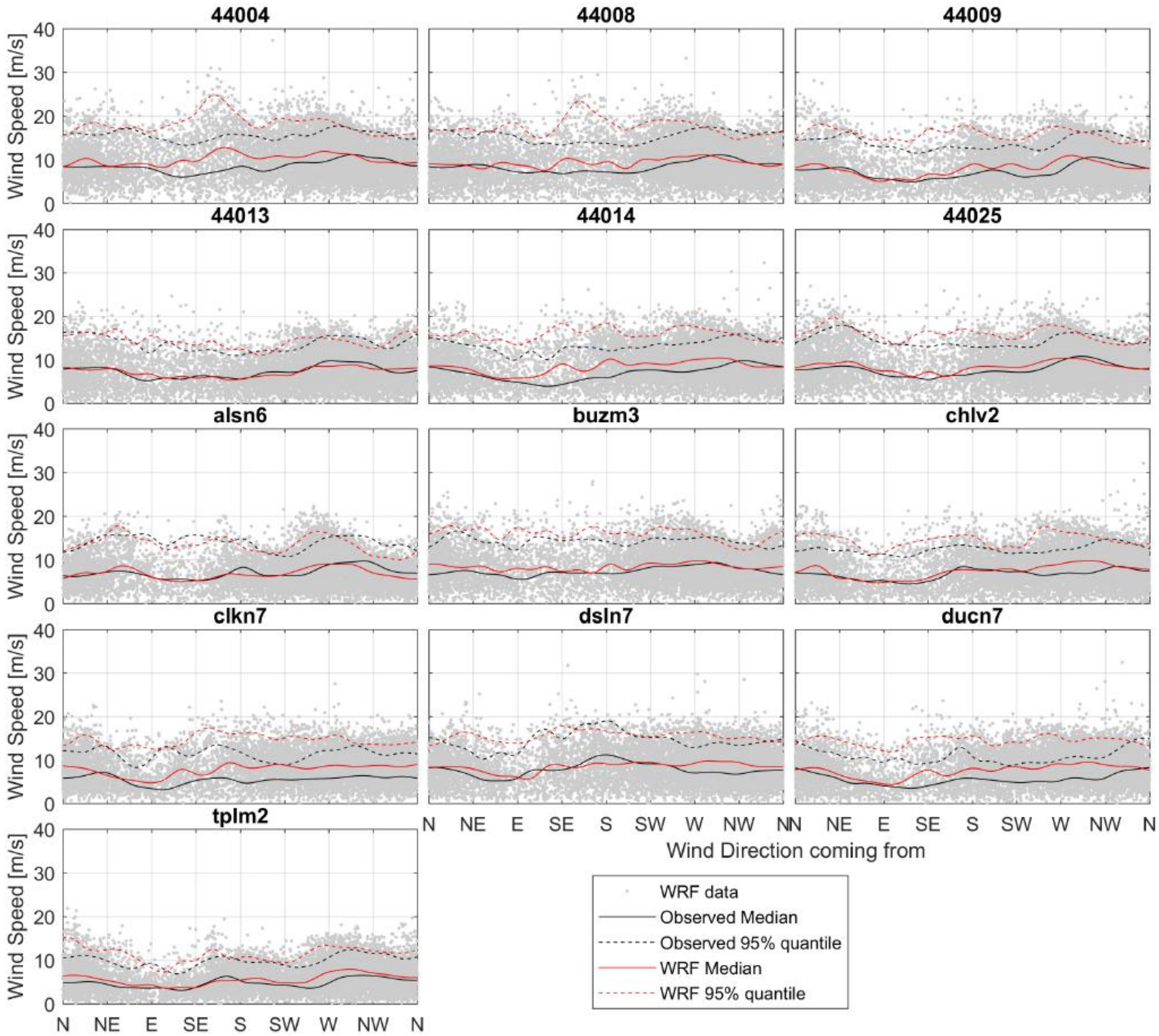

Figure S5. Same as Fig. S3 but for WRF-HadGEM.

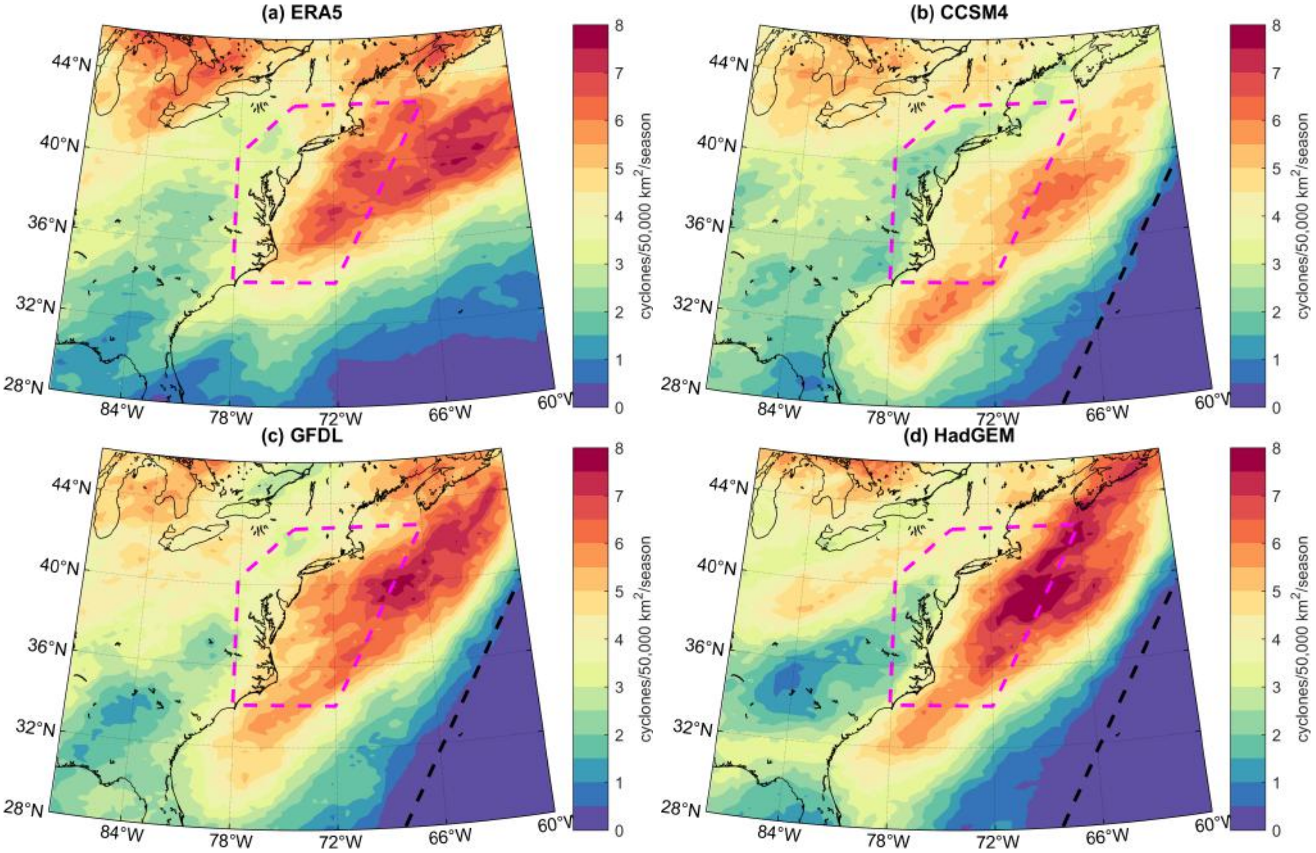

Figure S6. Spatial distribution of cool-season ETC density (number of cyclones per 50,000 km^2 per season) in the western North Atlantic Ocean during the historical decade (1995-2004) for: (a) ERA5 reanalysis data, and the WRF-based RCMs; (b) WRF-CCSM4, (c) WRF-GFDL, (d) WRF-HadGEM. Black dashed line indicates the edge of the WRF computational domains, explaining the zero density further offshore. Dashed magenta region indicates the NEC zone in which the distribution of ETC intensity is shown in Fig. S7.

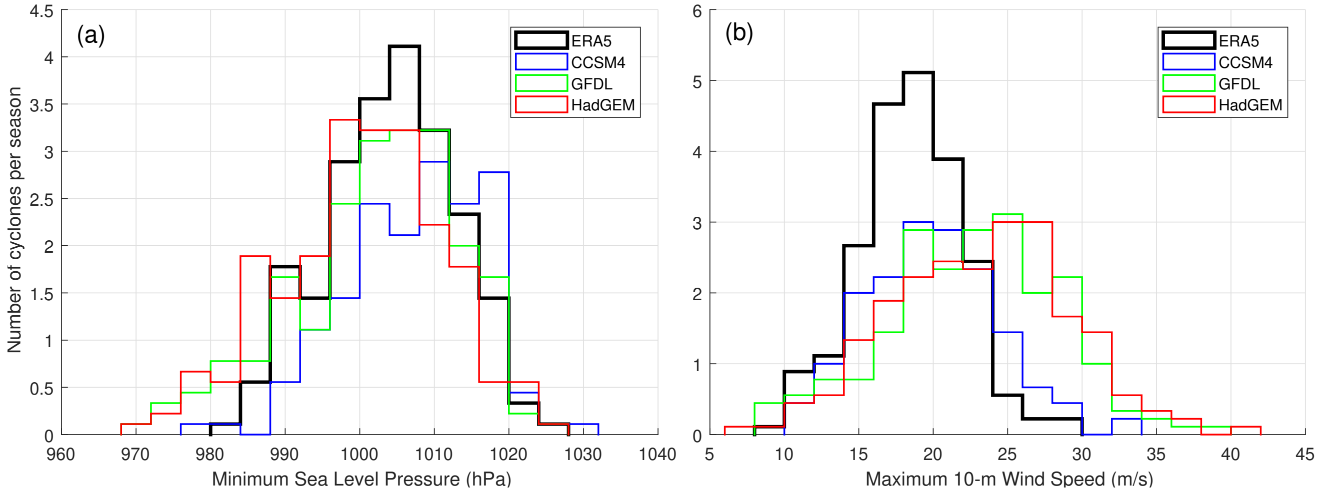

Figure S7. Distribution of the maximum lifecycle intensity of cool-season ETCs along the NEC (cyclones that fall within the magenta box region plotted in Fig. S6) during the historical decade (1995-2004) for ERA5 reanalysis data and the three RCMs (WRF-CCSM4, WRF-GFDL, WRF-HadGEM). (a) Minimum sea level pressure, (b) Maximum 10-m wind speed.